Crossover aspects in Ising strips under the influence of variable surface fields and a grain boundary

Z. Borjan
Faculty of Physics, University of Belgrade, P.O. Box 44, 11001 Belgrade, Serbia
(Received 6 August 2014; revised manuscript received 5 February 2015; published 12 March 2015)

I use an exact variational formulation of Mikheev and Fisher to study the critical Ising strip with a grain boundary and confining surfaces characterized by arbitrary and different surface magnetic fields. Energy density profiles that serve as order parameters of the system within the used method show strong nonmonotonous behavior in the vicinity of confining surfaces. I consider short-distance expansion of energy density profiles. New universal amplitudes associated with distant-wall corrections exhibit nontrivial crossover behaviors from positive to negative values as the field's variables are continuously varied. Casimir amplitudes calculated in a self-contained manner are characterized by complex manifolds which may comprise two disconnected positive wings separated by an area of negative values. I define and determine the generalized de Gennes-Fisher amplitude, which strongly suggests that a stress tensor is present within one of the distant-wall corrections. This is an unanticipated result given that a similar discovery for standard extraordinary (E) and ordinary (O) surface universality classes was based on the conformal invariance symmetry, which is *broken* under the present boundary conditions. A grain boundary essentially influences both energy density profiles and Casimir amplitudes, besides surface fields with a number of accompanying features that are examined in detail. We present closed analytic forms of energy density profiles for standard (N) and (O) BCs: $\varepsilon_{\rm NN}(x,g)$, $\varepsilon_{\rm OO}(x,g)$, $\varepsilon_{\rm NO}(x,g)$ [(N) is the *normal* surface universality class, g is the grain boundary's strength, x is the relative distance $x := z/L$ with L as a film width], thus enabling us to deduce their important symmetry properties and to have a detailed insight into their general behaviors.

DOI: 10.1103/PhysRevE.91.032121 PACS number(s): 05.70.Jk, 64.60.an, 64.60.De

I. INTRODUCTION

Usual critical behavior of confined thermodynamic systems may essentially change with respect to standard surface universality classes [1] such as the ordinary (O), the extraordinary (E), and the special or the "surface-bulk" (SB) one [2] when they are subjected to changeable boundary conditions (BCs) [3,4]. Manifestly different critical behavior of relevant universal quantities and laws governing them was also supported by experiments [5–7] referring to systems with tunable BCs. It turns out that systems driven from (O,E,SB) surface universality classes have very interesting and rich behavior in wide *crossover* regions situated among (O,E,SB) fixed points.

The underlying reason for more complex critical behavior in the case of adjustable BCs is the appearance of a new length scale that may become macroscopic and compete with the bulk correlation length ξ. Close to the (O) phase transition, when surface magnetic field h_1 is applied, the behavior of magnetization under the rescaling of distances is described by the relation [1]

$$m(z,t,h_1) \sim b^{-\beta/\nu} m\left(zb^{-1}, tb^{1/\nu}, h_1 b^{y_1^{\rm ord}}\right), \tag{1}$$

where $y_1^{\rm ord} = \Delta_1^{\rm ord}/\nu$ is a scaling dimension of h_1, β and ν are usual critical exponents associated with spontaneous magnetization and correlation length near the bulk critical temperature T_c, respectively, and $\Delta_1^{\rm ord}$ is the surface gap exponent at the ordinary phase transition [1]. In the case of $h_1 = 0$, letting $b \sim z$ in Eq. (1), magnetization takes on the scaling form $m \sim z^{-\beta/\nu}\mathcal{M}_t(z/\xi)$, with $\mathcal{M}_t(x)$ as a scaling function. I am currently interested in the situation at the bulk critical temperature $T = T_c$ and $h_1 \neq 0$. The scaling form of magnetization following from Eq. (1) in this case is

$$m(z,h_1) \sim z^{-\beta/\nu} m\left(z h_1^{1/y_1^{\rm ord}}\right). \tag{2}$$

The last equation implies that surface magnetic field h_1 induces the new length scale in the critical system:

$$l_1 \sim h_1^{-\nu/\Delta_1^{\rm ord}}. \tag{3}$$

As a consequence of (2), singular behavior of thermodynamic quantities may go through different universal regimes. For example, the short-distance behavior $z \ll l_1$ of magnetization is described by the law $m(z) \sim h_1 z^{\kappa}$, where $\kappa = (\Delta_1^{\rm ord} - \beta)/\nu$. In the opposite limit $z \gg l_1$ magnetization approaches the bulk equilibrium value zero as $z^{-\beta/\nu}$ [3].

The Casimir effect, originally discovered in electrodynamics, arises when confining surfaces influence the spectrum of electromagnetic fluctuations between them in a way that causes vacuum energy of the electromagnetic field to become size and shape dependent, which leads to attractive or repulsive force between them depending on the geometry involved. Near a critical point of a thermodynamic system the fluctuating field of order parameter becomes important, instead of the electromagnetic field. A field-theoretic interpretation of critical phenomena [8] explains that an analogous underlying mechanism causes boundaries in critical systems to play the same role as in electrodynamics. They modify the spectrum of the fluctuating order parameter so that the singular part of the free energy $\mathcal{F}^{\rm ex}(t,L)$ becomes dependent on separation distance L between the surfaces. Due to this a new force in the thermodynamic system occurs near the critical point, the Casimir force $-\partial\mathcal{F}^{\rm ex}/\partial L$ [8,9]. Tunable BCs may profoundly influence the Casimir effect in thermodynamic systems as well. The thermodynamic Casimir force $F_{\rm Cas}$ between the two

macroscopic parallel plates at a distance L decays as L^{-d} in the d-dimensional space at the bulk critical temperature T_c. The strengths of the Casimir force for standard (O,E,SB) BCs are determined by dimensionless Casimir amplitudes (CAs) Δ_{ab} [8], so that

$$F_{\rm Cas} = (d-1)\Delta_{ab}L^{-d}. \tag{4}$$

The universal constants Δ_{ab} may depend on the BCs denoted above by (ab).

It was shown that such a picture expressed by Eq. (4) is oversimplified in case of *variable* symmetry-preserving BCs [10]. It turns out that the Casimir force in this case cannot be characterized by constant amplitudes Δ_{ab}. Instead, Δ_{ab} become effective scale (i.e., L-) dependent amplitudes $\Delta_{c_1c_2} \to \mathcal{D}(c_1L^{\Phi/\nu},c_2L^{\Phi/\nu})$, where c_i $(i=1,2)$ are the so-called surface enhancements controlling surface properties [1], while Φ is the surface crossover exponent [1]. The study shows [10] that the nature of the Casimir force at the bulk critical point $T=T_c$ may change from repulsive to attractive and vice versa when BCs are smoothly varied.

The simultaneous influence of thermal and surface magnetic field effects on the Casimir force exclusively was studied by the transfer-matrix [11] and mean-field [12] methods. These results show that the strength as well as the sign of the force can be controlled by varying the temperature or the surface fields. They also point out that the Casimir force as a function of the temperature exhibits in the crossover regime between (N) and (O) BCs more than one extremum and for certain ranges of surface field strengths it changes sign twice upon varying temperature.

We clarify some important aspects of the rich crossover phenomena arising away from standard surface universality classes in the critical $(T=T_c)$ Ising strips under the confinement of surface fields h_i $(i=1,2)$, $h_1 \neq h_2$, $h_1h_2>0$. Additionally, I introduce grain boundary (GB) in the system and observe how tunable BCs and the GB as a model of internal defect influence at the same time the critical behavior of Ising strips. Our study uses the exact variational principle [13] as an alternative to detailed methods such as the transfer-matrix or Pffafian techniques, which may result in very complex expressions while further efforts are usually required to turn them into scaling forms and extract universal quantities.

We address specifically critical energy density profiles (EDPs) $\varepsilon(\vec{r})$ which, together with magnetization $m(\vec{r})$, are among primary local quantities in semi-infinite systems or films [1,8]. Energy density is closely related to the internal energy density $u(T,L)$ of the system via the relation $u(T,L) = \int_0^L \varepsilon(t,z,L)dz$. Magnetization m and energy density ε are conjugate variables with respect to the *fields* such as the reduced magnetic field $h = H/k_BT$ and the reduced temperature $t=(T-T_c)/T_c$, namely, $m=-\partial f_b/\partial h$, $\varepsilon = \partial f_b/\partial t$, where f_b is the Helmholtz free energy of the bulk thermodynamic system. All considerations [1,8] suggest that *local* observables such as the mean magnetization at a given point or local energy density are very sensitive to disturbances caused by the surface. Indeed, their thermodynamic averages near the surface tend to differ significantly from their values deep inside the bulk.

At the bulk critical point the z dependence of the scaling density profile $\langle\psi(\vec{r})\rangle_{\infty/2}$ in the corresponding semi-infinite system for *large* distances z from the wall is given by

$$\langle\psi(\vec{r}_{||},z)\rangle_{\infty/2} - \psi_b = A_\psi z^{-x_\psi}, \tag{5}$$

where $\langle\psi\rangle$ is either the magnetization m or energy density ε and ψ_b is the equilibrium bulk value of corresponding scaling density. A_ψ in Eq. (5) is a nonuniversal amplitude and x_ψ is scaling dimension given by $x_m=\beta/\nu$ for magnetization and by $x_\varepsilon=(1-\alpha)/\nu$ for energy density [1]. Critical exponent α is associated with singular behavior of specific heat near the bulk critical temperature T_c.

We explore first the *global* characteristics of EDPs in the film geometry, that is, the full form of the corresponding universal scaling functions. Apart from their general importance in the theory that I stress below, the knowledge of complete EDPs enables us to calculate the Casimir force within the present theoretical framework. The other aspect of our work examines small perturbation of the power law (5) due to the presence of the second wall at $z=L$. This is usually termed the *distant-wall correction* [8]. For example, in the case of standard (E) and (O) BCs, for three combinations $(\psi,a) = (\varepsilon,\mathrm{E})$, (ε,O), and (m,E), the corresponding film profile at small distances becomes

$$\langle\psi(z\ll L)\rangle = \langle\psi(z)\rangle_{\infty/2}\left[1+B_{ab}\left(\frac{z}{L}\right)^{d^\star}+\cdots\right], \tag{6}$$

where $\langle\psi(z)\rangle_{\infty/2}$ is given by Eq. (5) and $d^\star$ is spatial dimension $d^\star=d$ for $d<d_>$ and $d^\star=d_>$ for $d\geqslant d_>$, with $d_>$ as the upper critical dimension ($d_>=4$ for the present scope of problems within the Ising universality class). Values of the universal constants B_{ab} depend on the boundary conditions (ab) at both the near and the far walls, which are characterized by surface fields h_1 and h_2, respectively. It turns out that the *de Gennes-Fisher* (dGF) amplitude B_{ab} is a simple combination of the CAs Δ_{ab} and a new amplitude C_T for standard (E,O) BCs [14,15],

$$B_{ab} = C_T(d-1)\Delta_{ab}. \tag{7}$$

Examination of the *short-distance expansion* of type (6), which I carry out for variable BCs in Sec. III C, is generally one of the important aspects of the theory of confined critical systems. It has involved a number of universal amplitudes for various standard BCs such as those included in Eq. (7), the structure of which features fundamental aspects of the theory [8,15]. Apart from terms (6) and (7), there are other distant-wall corrections that may become leading asymptotic contributions within short-distance expansions, as I consider in Sec. III C.

As already emphasized above, the thermodynamic Casimir effect arises due to the fluctuating field of the order parameter. The induced Casimir effect in critical systems is described within this work by the fluctuating field of the EDP, which plays part as the order parameter, as will be clear from Sec. II. By examining short-distance expansions analogous to Eq. (6) for more general symmetry-breaking BCs, I have also *generalized* the dGF amplitude B_{ab} (7), which reveals another type of relation to CAs. This is another reason which makes the study of Casimir effect [8] necessary within the present framework, making the adopted formulation [13] complete regarding all its aspects.

While showing that global EDPs, CAs, and distant-wall corrections show interesting and nontrivial crossover behaviors, I also revisit some other fundamental theoretical questions pertinent to short-distance expansions such as Eq. (6). One of them is hyperuniversality of the amplitude analogous in our work to the amplitude C_T in Eq. (7), which was thoroughly examined in the past for standard BCs [16]. The other issue that I focus on for current BCs relates to the origin of the dGF amplitude (7) associated with the term $(z/L)^{d^*}$ in Eq. (6). Standard field-theoretic and conformal field approaches [8], used earlier to resolve this question for (E,O,SB) BCs, cannot be applied in the present situation.

Within the current work I also scrutinize Ising strips with the internal GB. The GB is an interface separating two bulk phases in a solid. It represents discontinuity in their physical or other characteristics. I study the concurrent influence of variable boundary surface fields h_1,h_2 and the GB onto critical EDPs and CAs characterizing Ising strips. While the GB as a model of a defect plane induces strong perturbations of the order parameter, it also influences essentially crossover behaviors of CAs. I show that it is possible to express the simultaneous influence of boundary surface fields and the GB within the unique CA. I outline here only some earlier pronounced results when the GB's influence is most closely related to critical systems. For example, the GB may induce melting by liquid upon approaching the melting curve [17]. Complete interfacial wetting of the GB by a liquidlike film within the mean-field theory of the two-dimensional lattice-gas model with short-range interactions was found [18].

The interface between two different bulk phases may be pinned (or localized) near the defect plane at low temperatures or may be depinned (or delocalized) at higher temperatures. In the case of identical bulk phases (say, $-$), separated by the GB, the $+$ phase may emerge and form microscopic wetting layers between the defect plane and either of the $-$ phases. No wetting phase transition may occur within the planar Ising model with the internal GB [19]. Yet, in case of the layered Ising model with GB, where systems on the two sides of the defect line are characterized by different couplings, the critical-point wetting (when interface is delocalized) may still be induced [20]. The same conclusion based on the real-space renormalization holds for three-dimensional systems [21].

The Landau theory of wetting in systems with GB enabled exact results [22], showing that systems of Ising universality class may undergo critical-point wetting only if the defect plane remains ordered at the critical temperature [therefore belonging to the (E) surface universality class]; otherwise, it is absent for (O) and (SB) BCs. The critical-point wetting may resemble the wetting at the free surface within a mean-field two-layered Ising model with the GB separating two semi-infinite systems [23].

When the interface of the planar Ising strip traverses internal GB at an angle, a new kind of phase transition from geodesic to the zigzag configuration takes place [24]. In connection with the same model, a specific mechanism of matter transport confined to the GB arises during relaxation of such system to its equilibrium [25].

In the context of nonequilibrium phase transitions, GBs, along with other extended spatial defects, like dislocations, may have dramatic effect on the prominent class of absorbing state transitions [26,27]. The absorbing state, featured by absence of fluctuations, is a dynamical trap which can be accessed with certain probability but cannot be left.

Let us mention the GB-segregation model which describes enrichment of a material constituent at the internal interface of the material such as the GB [28]. In connection with this, if the solidlike film condenses at a substrate, one observes layering when a monolayer or two or more layers may form. The completion of each layer occurs as a first-order transition accompanied by a jump in coverage. A series of layering transitions associated with the GB segregation was found in the lattice-gas model of a binary alloy [29].

When exploring systems with various inhomogeneities such as localized defects including walls, steps, interfaces between different phases, GBs, etc., it is crucial to know profiles of various densities in order to be able to calculate extensive thermodynamic quantities, such as specific heat, adsorption, etc. One of valuable approaches to such problems adopts variational formulation. The classical van der Waals-Landau-Ginzburg or the local mean-field theory [30] are among the most often used approaches of this kind. We calculate an inhomogeneous order parameter profile $m(\vec{r})$ induced by the arbitrary external field $h(\vec{r})$ within this theory from the *local* [31] free energy functional $\Omega[m] = \int dr\{\frac{1}{2}c|\nabla m|^2 - h(\vec{r})m(\vec{r}) + \frac{1}{2}t_0m^2(\vec{r}) + \frac{1}{4}um^4(\vec{r}) + \cdots\}$. Unfortunately, the van der Waals-Landau-Ginzburg functional $\Omega[m]$ fails to give correct description in the critical region below the upper critical dimension $d_>$.

Several *local* but approximate functionals $\tilde{\Omega}[t,m]$ have been proposed as generalizations [32,33] of van der Waals-Landau-Ginzburg functional $\Omega[m]$. Although very effective for a number of problems within finite systems such as the calculation of interfacial tensions [34], critical adsorption [35], Casimir force [36], it also contains flaws. Yet, when addressing, for example, the wall free energy of the near critical system *above* the bulk critical temperature T_c or the local perturbations to the bulk produced by a wall or an interface for (O) or (OO) BCs the above free energy functionals $\Omega[m]$ or $\tilde{\Omega}[t,m]$ defined only by the order parameter $m(\vec{r})$ do not suffice as the order parameter for (O) and (SB) BCs becomes zero for $T \geqslant T_c$. Then energy density $\varepsilon(\vec{r})$, in fact, provides singular contributions to thermodynamic quantities. This is the case in physical situations specified by symmetry-preserving BCs such as ^{4}He near the λ point of transition to superfluidity when (OO) BCs are relevant. Similarly, the above mentioned concept based on the use of the *single* order parameter $m(\vec{r})$ may be inefficient for GBs and surfaces in ferromagnetic materials in the zero field.

To overcome this deficiency an entropylike thermodynamic potential $\mathcal{S}[m,\varepsilon]$, which I use presently, has been defined as the functional of *both* local magnetization and local energy density [13]. More profound theoretical arguments related to the scaling theory and the renormalization group analysis suggest that a correct description should include all relevant critical densities with scaling dimensions $x_m = \beta/\nu, x_\varepsilon = (1-\alpha)/\nu, \ldots < d$ [37]. In the case of the Ising universality class only m and ε are necessary. Such models treat the two scaling densities m and ε on the same footing.

The paper is organized as follows. In Sec. II I explain the main features of the model [13] used in this work. I discuss

BCs that model the boundary "surfaces" of the Ising strip characterized by continually variable surface magnetic field variables. I further comment on the model of the GB applied to the current formulation. Section II is completed with a general formula of CAs used in Secs. III and IV. I proceed with Sec. III, which considers the Ising strip with changing surface field variables and without an internal defect line. I analyze exact EDPs, as the order parameter of the system, CAs, as well as short-distance expansion of EDPs $\varepsilon(x,y_1,y_2)$ in detail. In close relation to the latter I present the distant-wall correction universal amplitudes and discuss a number of essential questions, including that of an important dGF universal amplitude. Section IV generalizes earlier findings in a more complex situation when the Ising strip with varying boundary surface fields also accommodates an internal defect line. I explore coexisting influences of surface fields and the GB onto the EDPs and CAs exhaustively and compare these results with those of Sec. III. Several special cases of physical interest are (NN), (OO), and (NO) BCs with the internal GB, allowing for a number of analytic insights providing valuable and useful symmetry properties, among other results.

II. THEORETICAL BACKGROUND

In order to explore crossover behaviors among standard surface universality classes, a "microcanonical" or an entropy functional $\mathcal{S}[\varepsilon(\vec{r}),m(\vec{r})]$ was established [13], where $m(\vec{r})$ is the order parameter and $\varepsilon(\vec{r})$ local energy density. Such functionals yield the free energy functional $\mathcal{F}$ via $\min_{\varepsilon(\vec{r}),m(\vec{r})}\{\mathcal{S}[\varepsilon,m]-\int d\vec{r}[t\varepsilon+hm]\}$, from where it is possible to calculate straightforwardly $\varepsilon(\vec{r})$, as well as other quantities. This idea was first realized for the one-dimensional nearest-neighbor ferromagnetic Ising chain. Expressions for the functional $\mathcal{S}[\varepsilon,m]$ have been derived in a discrete, lattice formulation and then in the scaling limit as the conformally covariant local functional $\mathcal{S}_1=\frac{1}{2}\int dz\varepsilon(z)\{\ln\frac{1}{2}\varepsilon(z)+\mathcal{B}[m;\dot{m}/\varepsilon]\}$, with $\mathcal{B}(u,v)=\frac{1}{2}\ln[(1+v)^{1+v}(1-v)^{1-v}/\exp(2)(1-u^2)]$, $\dot{m}:=dm/dz$ [37]. The result on the one-dimensional $\mathcal{S}_1$ can be further used to find the *exact* variational functional for the two-dimensional, layered Ising model in the zero field ($h=0$). The advantages of continuum over lattice formulation include that (a) it represents the whole Ising universality class instead of only the nearest-neighbor model, (b) it is manifestly conformally covariant, and (c) results are directly available in a scaling limit.

By treating the two-dimensional Ising model as a set of independent $d=1$ Ising chains denoted by wave vectors $q\in[0,\pi]$ it was possible to formulate an exact free energy functional in terms of free energy $\mathcal{F}_1$ of individual chains as $\mathcal{F}_{d=2}=\int_0^\pi\frac{dq}{2\pi}\mathcal{F}_1[\tau_q;H_q]$. Each chain in the last equation is defined by spatially varying coupling τ_q in the external magnetic field H_q, and $\mathcal{F}_1=\min_{\mathcal{E}_q,\mathcal{M}_q}\{\mathcal{S}_1[\mathcal{E}_q,\mathcal{M}_q]-\int dz[\tau_q(z)\mathcal{E}_q(z)+H_q(z)\mathcal{M}_q(z)]\}$. Variational parameters $\mathcal{E}_q$ and $\mathcal{M}_q$ play the role of spatially varying energy and magnetization densities, respectively, of the one-dimensional chain labeled q. This way the basic, zero-field thermodynamic potential $\mathcal{F}_{d=2}$ of the two-dimensional layered Ising model decouples exactly into a sum of potentials relevant to the set of one-dimensional Ising chains denoted by the wave number q. The full free energy follows after minimization [13] with respect to $\mathcal{E}_q$,

$$\mathcal{F}_2[\varepsilon_q(z)]=\min_{\varepsilon_q(z)}k_bT\int_0^\Lambda\frac{dq}{2\pi}\int dz[\mathcal{L}_q(\varepsilon_q,\dot{\varepsilon}_q)-t(z)\varepsilon_q], \tag{8a}$$

$$\mathcal{L}_q(\varepsilon_q,\dot{\varepsilon}_q):=-E_q(\varepsilon_q,\dot{\varepsilon}_q)+\frac{1}{2}\dot{\varepsilon}_q\tanh^{-1}\left(\frac{\dot{\varepsilon}_q}{2E_q}\right), \tag{8b}$$

$$E_q(\varepsilon_q,\dot{\varepsilon}_q)=\sqrt{\frac{1}{4}\dot{\varepsilon}_q^2+q^2\left(1-\varepsilon_q^2\right)}, \tag{8c}$$

where ε_q in the above equations specify energy modes of layers of the original two-dimensional Ising model, $\dot{\varepsilon}_q:=d\varepsilon_q/dz$, and $t(z)$ is the basic thermal field.

Functional (8) should be used in the scaling limit near the critical point. In order to consider finite-size systems, this functional comes with additional surface terms,

$$\mathcal{L}_{S,q}^{(i)}=\left\{-g_i\varepsilon_q(z_i)+\tfrac{1}{4}[1+\varepsilon_q(z_i)]\ln[1+\varepsilon_q(z_i)]+\tfrac{1}{4}[1-\varepsilon_q(z_i)]\ln[1-\varepsilon_q(z_i)]\right\}\delta(z_i),\quad i=1,2, \tag{9}$$

where $z_1=z$ and $z_2=L-z$, when boundary "surfaces" are situated at $z=0$ and $z=L$. The first term in Eq. (9) describes interaction with the surface field. By employing scaling ideas it follows [13] that $g_i\approx\frac{1}{2}\ln(q/h_i^2), i=1,2$. Boundary terms (9) come from the scaling limit of the original lattice Ising model.

The general solution to the Euler-Lagrange equation of functional (8) at bulk criticality is

$$\varepsilon_q(z)=\frac{1}{\sinh(2Lq)}\sum_{i=1}^{2}\varepsilon_q^{(i)}\sinh(2q\tilde{z}_i), \tag{10}$$

where $\tilde{z}_1=L-z$ and $\tilde{z}_2=z$, and wall energy modes $\varepsilon_q^{(1)}=\varepsilon_q(z=0)$ and $\varepsilon_q^{(2)}=\varepsilon_q(z=L)$ follow from the system of the following two equations deriving from minimizing surface boundary terms (9):

$$\mathrm{sgn}(-i+3/2)p_q(x_i)-g_i-\frac{1}{4}\ln\left(\frac{1+\varepsilon_q^{(i)}}{1-\varepsilon_q^{(i)}}\right)=0,\quad i=1,2. \tag{11}$$

The last system of equations uses the definition of conjugate momenta to the "coordinates" ε_q, $p_q:=\partial\mathcal{L}_q/\partial\dot{\varepsilon}_q=\frac{1}{2}\tanh^{-1}[\dot{\varepsilon}_q/2E_q(\varepsilon_q,\dot{\varepsilon}_q)]$, where above $x_1=0,x_2=L$.

Knowing energy density modes ε_q local EDPs are calculated by

$$\varepsilon(x=z/L,y_1,y_2)=\int_0^\infty\frac{dq}{2\pi}\varepsilon_q(x,y_1,y_2), \tag{12}$$

where $y_i:=D^2h_i^2L$, $(i=1,2)$, D is a nonuniversal metrical factor $D=e^{K_c}\sqrt{2/a}$, $K_c=\ln[1+\sqrt{2}]/2$, which is used to set up complete equivalence with the microscopic model.

Within the study of critical behavior of inhomogeneous thermodynamic systems defined by the above arbitrary symmetry-breaking BCs, I consider the overall features of universal functions of their scaling densities such as EDPs. Indeed, addressing EDPs under the influence of various BCs [8,14,38–41] is a lasting effort in the theory of critical phenomena. Knowing profiles $\varepsilon_q(z)$, other relevant physical quantities characterizing inhomogeneities due to surfaces, films, chains, and GBs, such as specific heat, adsorption, etc.,

may be calculated from the free-energy functional $\mathcal{F}$. At the same time, complemental information on shared influence of BCs on scaling densities derives from their short-distance expansions [1,8,16,32,39], such as Eq. (6), leading to formulation of several important universal amplitudes, such as B_{ab} and C_T in Eq. (7), which were scrutinized in the past.

Examining *local* characteristics of EDPs within the present work I have recognized that the structure of one of the distant-wall corrections is closely related to CA $\Delta(y_1,y_2)$ for BCs under consideration. Thus, it became necessary to study the Casimir force and derive CA within the existing theoretical framework. To incorporate the study of CA under the impact of surface fields h_i ($i = 1,2$), we need a *finite-size* term [8,32] of the functional (8):

$$\mathcal{F}_2^{\rm ex} = \min_{\varepsilon_q(z)} k_b T \int_0^{\Lambda} \frac{dq}{2\pi} \int_0^L dz[\mathcal{L}_q(\varepsilon_q,\dot{\varepsilon}_q) + q]. \tag{13}$$

The thermodynamic Casimir force is defined as a generalized force conjugate to separation L between the confining boundaries [8,32] $F_{\rm Cas} = -\partial\mathcal{F}_2/\partial L$. I simplify the calculation of CA with the relation [42] $\partial\mathcal{F}_2^{\rm ex}/\partial L + E^{\rm ex} = 0$, which amounts to the Hamilton-Jacobi equation in the mechanical analog, where $E^{\rm ex}$ is the total conserved energy of the system at $T = T_c$. The energy $E^{\rm ex}$ follows from the formula $E^{\rm ex} = \int \frac{dq}{2\pi} E_q^{\rm ex}$, with $E_q^{\rm ex} = E_q - q$ and E_q given by Eq. (8c). According to the finite-size scaling arguments [8,32], the critical Casimir force is given by the law

$$F_{\rm Cas} = L^{-d}(d-1)\Delta(y_1,y_2), \tag{14}$$

with $d = 2$ presently and $\Delta(y_1,y_2)$ equivalent to CAs Δ_{ab} (4) for standard BCs (NN), (NO), (OO), etc. [8] [where N denotes *normal* surface universality class equivalent to the (E), which itself cannot exist in $d = 2$]. After solving Eqs. (11) we obtain E_q and $E_q^{\rm ex}$ from Eqs. (10) and (8c). Then, from the above Hamilton-Jacobi like equation and Eq. (14) we set up the general formula for CA defined by simultaneous influence of the surface fields:

$$\begin{aligned}\Delta(y_1,y_2) &= \int_0^{\infty} \frac{dt}{2\pi} E^{\rm ex}_{t=qL} \\ &= \int_0^{\infty} \frac{dt}{2\pi} \left\{ \frac{1}{2}\sqrt{4t^2\left[1-\varepsilon_q^2(x)\right] + \dot{\varepsilon}_q^2(x)} - t \right\}. \end{aligned} \tag{15}$$

The GB (situated at $z = 0$) is introduced in the present model [13] with the thermal field $t(z)$ of Eq. (8) adding the δ function character to the simplest model of the boundary as a stepwise variation of the basic field $t_-\theta(-z) + t_+\theta(z)$, that is [13],

$$t(z) = t_-\theta(-z) + t_+\theta(z) + g\delta(0). \tag{16}$$

We recall that the temperaturelike thermal field $t(\vec{r})$ embodies a variation of the coupling constant $J(\vec{r})$ of the original lattice Ising model, $t(\vec{r}) = K_c - K(\vec{r})$, where $K(\vec{r}) = J(\vec{r})/k_BT$, while K_c is the bulk critical value of K. Such a model enables the desirable limit of the microscopic model when both lattice spacings $a_{\perp+}$ and $a_{\perp-}$ on the two sides of the GB together with the interface width approach zero (see Fig. 1 and other details in Ref. [13]). Then, in addition to BCs (11) (now formulated at boundaries situated at $z_1 = -L/2$ and $z_2 = L/2$), I also deal with the third one for the GB at $z = 0$ that follows after minimizing the functional (8):

$$p_q(0+) - p_q(0-) = -g. \tag{17}$$

The long-wavelength limit of the exact lattice functional [13], which preceded continuum formulation (8) confirmed correctness of the GB model (16). The GB of the type (16) makes each mode $\varepsilon_q(z)$ continuous through $z = 0$; that is, it holds $\varepsilon_q(0+) = \varepsilon_q(0-)$, but $\dot{\varepsilon}_q(z)$ is discontinuous, which reflects in the jump of the canonical momentum $p_q(z)$ of Eq. (17). One should comprehend the field g, defined by Eq. (16), as the measure of strength K_0 of boundary bonds coupling domains on two sides of the GB (see Fig. 2 and the accompanying discussion in Ref. [13]). I comment on important limits $g \to \pm\infty$ in Sec. IV.

III. THE ISING STRIP: ADAPTABLE SURFACE FIELDS

I study in this section, as the first step, EDPs and CAs of the Ising strip exposed only to changing BCs delineated by surface field variables y_1 and y_2. Apart from discussing their crossover behaviors, I also go over the short-distance expansion of the EDP analogous to Eq. (6). Because it is more complicated for new BCs than Eq. (6) it enables us to determine several universal amplitudes associated with the distant-wall corrections, such as generalized dGF amplitude B_{ab}, originally introduced by Eqs. (6) and (7). Furthermore, I generalize my considerations in the next section allowing that the internal defect line is present in the strip besides existing surface fields.

A. Global energy density profiles

We solve the system of nonlinear equations (11) in the general case of BCs $h_1 \neq h_2$, obtaining for surface energy modes $\varepsilon_q^{(1)}$ and $\varepsilon_q^{(2)}$

$$\varepsilon_q^{(1)} = \frac{[-1 + e^{2(g_1+g_2)}]\cosh(Lq) + (e^{2g_1} - e^{2g_2})\sinh(Lq)}{[1 + e^{2(g_1+g_2)}]\cosh(Lq) + (e^{2g_1} + e^{2g_2})\sinh(Lq)}, \tag{18a}$$

$$\varepsilon_q^{(2)} = \frac{\cosh(Lq)(-1 + e^{2g_1+2g_2}) + (-e^{2g_1} + e^{2g_2})\sinh(Lq)}{\cosh(Lq)[1 + e^{2g_1+2g_2}] + (e^{2g_1} + e^{2g_2})\sinh(Lq)}. \tag{18b}$$

Using the last solution in Eq. (10), we determine the energy density modes $\varepsilon_q(z)$:

$$\varepsilon_q(x) = \frac{\operatorname{csch}(2t)\{(t^2 - y_1y_2)\cosh[t(1-2x)]\sinh(2t) + t(y_1 - y_2)\sinh(t)[\sinh[2t(x-1)] + \sinh(2tx)]\}}{(t^2 + y_1y_2)\cosh(t) + t(y_1 + y_2)\sinh(t)}. \tag{19}$$

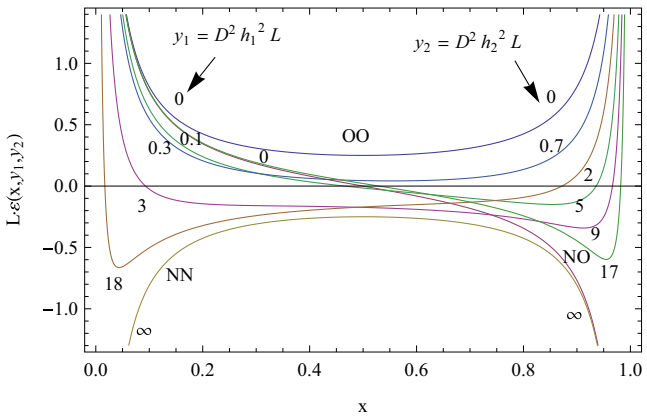

FIG. 1. (Color online) Plots of the universal part of EDPs $\varepsilon(x,y_1,y_2)$ with respect to variables $x = z/L$, $y_1 = D^2h_1^2L$, and $y_2 = D^2h_2^2L$ confined to a two-dimensional Ising strip of width L for $h_1 \neq h_2$ ($h_1h_2 > 0$). Curves in the picture correspond to the following values of surface fields variables: $(y_1,y_2) = (0,0)$, $(0,\infty)$, (∞,∞), $(0.1,5)$, $(0.3,0.7)$, $(3,9)$, $(18,2)$, $(0,17)$. The first three couples of values correspond to (OO), (ON), and (NN) BCs, respectively.

Figure 1 presents EDPs $\varepsilon(x,y_1,y_2)$ confined to critical Ising strips obtained by integrating $\varepsilon_q(z)$ from Eq. (19) according to Eq. (12) for several arbitrarily assigned values of field variables y_1 and y_2. Pronounced nonmonotonous behavior that may accommodate one or two different minima near confining "surfaces" and a single maximum located somewhere in between them distinguishes EDPs for a range of field variables y_1 and y_2. For larger values of field variables y_1 and y_2 minima of energy density curves evolve towards surfaces, with a general tendency to collapse onto the surfaces when $y_1 \to +\infty$ and/or $y_2 \to +\infty$, transforming into monotonous diverging behavior. Similar behavior occurs when surface field variables y_1 and y_2 attain very small values, that is, $y_1 \to 0$ and/or $y_2 \to 0$, except that in this case curves diverge upward $\varepsilon(x) \to +\infty$ as $x \to 0$, that is, opposite to a previous case. Figure 1 also shows EDPs in limits $(y_1 \to +\infty, y_2 \to +\infty)$, $(y_1 \to 0, y_2 \to 0)$, and $(y_1 \to +\infty, y_2 \to 0)$ with additional designations (NN), (OO), and (NO), respectively.

We extract a leading influence of the nearest wall on EDPs by scrutinizing only a part of EDPs pertaining to a single wall. Then the system of Eqs. (11) decouples, yielding EDPs in a closed form,

$$\varepsilon_{\infty/2}(z,h_1) = \frac{1 - 4e^{2h_1^2 z} h_1^2 z \Gamma\left[0, 2h_1^2 z\right]}{4\pi z}, \tag{20}$$

where $\Gamma[a,z] := \int_z^\infty t^{a-1}e^{-t}dt$ is an incomplete gamma function. We solve the equation of extremum $\dot{\varepsilon}_{\infty/2}(z^\star,h_1) = 0$, that is, $1 - 4h_1^2z^\star + 8e^{2h_1^2z^\star}h_1^2z^\star\Gamma[0,2h_1^2z^\star] = 0$, numerically for assigned values of the surface fields $h_i^{(k)}, k = 1,2,\ldots$. As an example, for an ascending array of fields values $h_1^{(1)} = 0.5$, $h_1^{(2)} = 2.0$, and $h_1^{(3)} = 4.0$ we have from the last equation the descending array for coordinates $z_k^\star$ of extreme points of EDPs: $z_1^\star = 3.12$, $z_2^\star = 0.195$, and $z_3^\star = 0.0487$, respectively, demonstrating that for larger values of surface fields curves' minima are approaching the walls, while their amplitudes get larger. As a matter of fact, $z_k^\star, k = 1,2,\ldots$ mark the *new* characteristic length l_1 (3) in the system, besides the film width L, clearly pointing out to a crossover of EDPs from descending to ascending behavior and therefore inducing nonmonotonicity of pertinent quantities. Nonmonotonicity of EDPs as functions of the surface field has been also reported in the case of the *semi-infinite* geometry for $T > T_c$ [13].

We now show that Eqs. (19) and (12) embody former results on EDPs $\varepsilon_{ab}(x)$ for standard (N) and (O) surface universality classes. Carrying out limits $y_1,y_2 \to \infty$ and $y_1,y_2 \to 0$ in Eq. (19), we get $\varepsilon_q^{aa}(x) = A_a \cosh[t(1-2x)][\cosh(t)]^{-1}$, where a =(N,O), $A_N = -1$, $A_O = 1$. An integration of the last expression by Eq. (12) yields [41] $\varepsilon_{aa}(x) = \tilde{A}_a/\sin(\pi x)$, with nonuniversal amplitudes of opposite signs, $\tilde{A}_N = -1/(4L)$ and $\tilde{A}_O = 1/(4L)$, implying

$$\varepsilon_q^{NN}(x) = -\varepsilon_q^{OO}(x), \quad \varepsilon_{NN}(x) = -\varepsilon_{OO}(x). \tag{21}$$

The last relationship between profiles $\varepsilon_{NN}(x)$ and $\varepsilon_{OO}(x)$ conforms to inverted curves for (NN) and (OO) BCs in Fig. 1. Similarly, realizing limits $y_1 \to 0$, $y_2 \to \infty$ in Eq. (19) give $\varepsilon_q^{ON}(x) = -\mathrm{csch}(2t)\{\sinh[2t(x-1)] + \sinh(2tx)\}$, so that after integration (12) we have $\varepsilon_{ON} = \cot(\pi x)/(4L)$, which is the EDP for *mixed* BCs [14].

B. Casimir force

We establish the formula for CA in the general case of freely variant surface fields $h_1 \neq h_2$ ($h_1h_1 > 0$) by replacing the solution (19) into Eq. (15):

$$\Delta(y_1,y_2) = \int_0^\infty dx \underbrace{\frac{x}{2\pi} \frac{\exp(-x)(y_1-x)(-y_2+x)}{[(y_1y_2+x^2)\cosh x + (y_1+y_2)x\sinh x]}}_{\Delta^{(k)}(y_1,y_2,x)}. \tag{22}$$

The last variational result agrees with the off-critical transfer-matrix calculations of Ref. [11] in the limit $T \to T_c$. In Fig. 2 I show a distinctive feature of CA $\Delta(y_1,y_2)$, which is that it not only varies in magnitude but it may also change twice the nature of the Casimir force from *repulsive* to *attractive* and vice versa with smooth variation of field variables y_1 and y_2 along certain trajectories. The possibility to tune the Casimir force and change its nature from repulsive to attractive only by altering surface fields in *higher dimensions* ($d > 2$) follows from Monte Carlo simulation analysis [43] in $d = 3$ in special cases of (E,h_1) and $(h_1,|h_1|)$ BCs as well as from the mean-field analysis ($d \geqslant 4$) realized for several preselected cases [12].

Equation (22) encompasses earlier results for standard surface universality classes. Taking limits $y_1,y_2 \to \infty$ and $y_1,y_2 \to 0$ in Eq. (22) results in the same formula $\Delta_{NN} = \Delta_{OO} = \int_0^\infty \frac{xdx}{2\pi}(\tanh x - 1) = -\pi/48$, also known from other approaches for [44] (OO) and [42] (NN) BCs. The equality of CAs $\Delta_{NN} = \Delta_{OO}$ stems from a symmetry property (21) between EDPs for (NN) and (OO) BCs. CA for *mixed* (NO) BC is retrieved from Eq. (22) in limits $y_1 \to \infty$, $y_2 \to 0$, giving [45] $\Delta_{NO} = \int_0^\infty \frac{xdx}{2\pi}(\coth x - 1) = \pi/24$.

Complementary but different analysis [10] of crossover behavior of CA for *symmetry-preserving* BCs in dimension

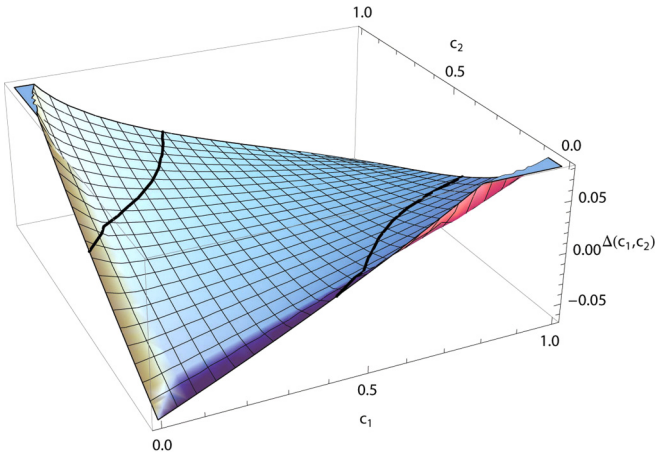

FIG. 2. (Color online) Generalized CA $\Delta(c_1,c_2)$ [$c_i := y_i/(1+y_i)$], $y_i := (Dh_i)^2 L, (i=1,2)$ defined by $h_1 \neq h_2, h_1 h_2 > 0$ for Ising universality class in $d=2$ according to Eq. (22). The quantity $\Delta(c_1,c_2)$ changes from *positive* values to *negative* ones and vice versa for some trajectories in the (c_1,c_2) space. Regions of the repulsive Casimir force are delimited by bold lines from the one where the Casimir force is attractive.

$d = 4-\varepsilon$ also highlights a possibility for CA to change both its nature and magnitude continuously varying BCs.

C. The short-distance expansion

In a film of thickness L the second wall is present at $z=L$. Examining scaling density profiles such as magnetization m or energy density ε near the first wall, i.e., for $z \ll L$, one notices the influence of the second wall at $z=L$ as a small perturbation of the power law (5). Additional terms such as $B_{ab}x^{d^\star}$ in Eq. (6) are called distant-wall corrections that I now examine due to the presence of the wall characterized by the arbitrary surface field variable y_2 at the distance L from the first wall featured by the variable field variable y_1. Here we need a more general discussion of the short-distance expansion originally introduced by Eq. (6). The common origin of the short-distance expansion about the surface for a given pair (ψ,a) [1] is

$$\psi(\vec{r}_{||},z)/\langle\psi(\vec{r}_{||},z)\rangle_{\infty/2} = 1 + \sigma_I(\vec{r}_{||})z^{x_\psi^{(S)}}C_1 + \cdots, \qquad (23)$$

where $(\psi,a) = (\varepsilon,\mathrm{O}),(\varepsilon,\mathrm{SB}),(\varepsilon,\mathrm{E}),(\phi,\mathrm{E})$, ϕ is the order parameter so that its average is magnetization $\langle\phi\rangle = m$ and $x_\psi^{(S)}$ is the surface exponent corresponding to the close wall ($z=0$). In the last equation the sequence σ_I, $\sigma_{II},\ldots,$ represents fluctuating local surface densities ("surface operators") [8].

It is an outstanding feature that all three cases (ε,O), (ε,E), and (ϕ,E), except $(\varepsilon,\mathrm{SB})$, are characterized by the surface exponent equal to the spatial dimension d [1,39],

$$x_\psi^{(S)} = d. \qquad (24)$$

The last equation indicates that the scaling dimension of the operator σ_I in Eq. (23) is d. It is intriguing that $x_\psi^{(S)}$ and σ_I are unique for the above mentioned cases, although generally they may differ for different pairs (ψ,a). This suggests that σ_I's have a common origin. It was argued that σ_I is related to the stress-tensor component $T_{\perp\perp}$ perpendicular to the surface [16],

$$\sigma_I(\vec{r}_{||}) = -\lim_{z\to 0} T_{\perp\perp}(\vec{r}_{||},z). \qquad (25)$$

The last equation is connected with the fact that the stress-energy tensor T_{kl} of the critical field theory is a bulk operator described by the scaling dimension d. It was also found that the amplitude $C_1 = C_T$ in Eq. (23) is related to the stress tensor correlation function in the half space at T_c:

$$C_T \big/ x_\psi^{(S)} \sim 1 \big/ [\lim\langle T_{\perp\perp}(\vec{r}_{||},z)T_{\perp\perp}(\vec{r}_{||},z')\rangle |\vec{r}_{||} - \vec{r}'_{||}|^{2d}].$$

For the critical film ($T=T_c$) with standard BCs the average of $T_{\perp\perp}$ equals [46]

$$\langle T_{\perp\perp}\rangle = (d-1)\Delta_{ab}L^{-d}. \qquad (26)$$

Equations (23)–(26) establish Eqs. (6) and (7), which are valid as the leading asymptotic contribution for (ε,O), (ε,E), and (ϕ,E) pairs of (ψ,a).

For $(\varepsilon,\mathrm{SB})$ the surface exponent $x_\psi^{(S)}$ in Eq. (23) is smaller than d,

$$\left[x_\varepsilon^{(S)}\right]_{\mathrm{SB}} = d - 1 - \Phi/\nu, \qquad (27)$$

where Φ is the crossover exponent [1] of the multicritical SB transition. Thus, Eqs. (24) and (25) do not apply in this case. Yet, Eq. (25) is present within the short-distance expansion (23) as the subleading contribution with the same structure given by Eqs. (6) and (7).

Expanding the EDP $\varepsilon(x,y_1,y_2)$ by means of Eqs. (19) and (12), with usual normalization with respect to semi-infinite profiles (20) $\varepsilon_{\infty/2}(z,h_1)$, we find

$$\frac{\varepsilon(x,y_1,y_2)}{\varepsilon_{\infty/2}(z,h_1)} = 1 + x\mathcal{C}(y_1,y_2) + x^2\int_0^\infty \tilde{\mathcal{D}}(y_1,t)\Delta^{(k)}(y_1,y_2,t)dt + \cdots, \qquad (28)$$

$$\mathcal{C}(y_1,y_2) = \int_0^\infty \frac{8ty_1(t-y_2)}{(t+y_1)[(t-y_1)(t-y_2)+e^{2t}(t+y_1)(t+y_2)]}dt, \qquad (29)$$

$$\tilde{\mathcal{D}}(y_1,t) = \gamma_S\mathcal{D}(y_1,t), \quad \mathcal{D}(y_1,t) = -\frac{8\pi\left(t^2+y_1^2\right)}{t^2-y_1^2}, \qquad (30)$$

with $\Delta^{(k)}(y_1,y_2,t)$ as an integrand of the integral formula (22) of CA. In the last equation $\gamma_s = 1$ for all $y_1 < +\infty$ and $\gamma_s = -1$ only for $y_1 \to \infty$, associated with different limits of the function $\varepsilon_{\infty/2}(z,h_1)$ (20): $z\varepsilon_{\infty/2}(z,h_1) \to 1/(4\pi)$ when $z\to 0$, $y_1 < \infty$ and $z\varepsilon_{\infty/2}(z,h_1) \to -1/(4\pi)$ when $z\to 0$, $y_1 \to \infty$. Figure 3 discloses intricate behavior of the distant-wall correction universal amplitude $\mathcal{C}(y_1,y_2)$, which may attain positive values (when the other wall enhances the profiles) and negative ones (when the distant wall makes the profiles weaker). Figure 4 features the second distant-wall correction of Eq. (28), which, similarly to the previous one, exhibits the alteration of its magnitude and sign. Figure 3 apparently points to the line of special values of the surface field variables

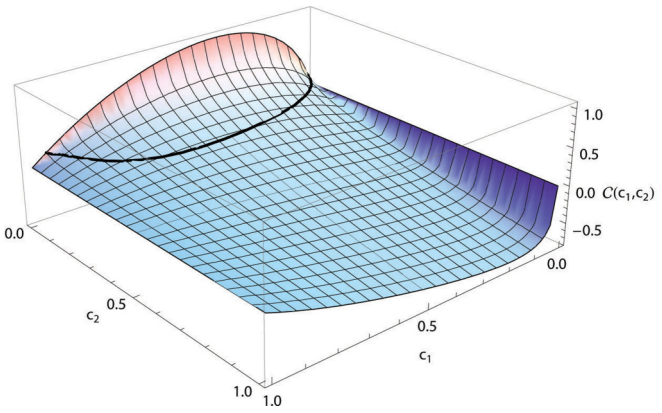

FIG. 3. (Color online) Crossover behavior of the leading distant-wall correction universal amplitude (29) $\mathcal{C}(y_1,y_2)$ of the short-distance expansion, Eq. (28). Areas of positive values (when EDPs are magnified by the distant wall) are delimited by the bold line from the negative ones (when the distant wall diminishes the EDPs).

$(y_1^\star, y_2^\star)$ defined by $\mathcal{C}(y_1^\star, y_2^\star) = 0$ [with the addition of (NN), (NO), and (OO) fixed points] along which the second distant-wall correction in Eq. (28) becomes the leading asymptotic contribution in the short-distance expansion of EDPs.

The last distant-wall correction of Eq. (28) incorporates standard (NN), (NO), and (OO) BCs: $\lim_{y_1\to\infty}\tilde{\mathcal{D}}(y_1,t) = \lim_{y_1\to 0}\tilde{\mathcal{D}}(y_1,t) \equiv C_T = -8\pi$, with the amplitude C_T hyperuniversal in $d = 2$ with respect to standard surface universality classes as earlier established in Ref. [16]. Combining the above fixed points' BCs, I have from Eqs. (28), (30), and (22) terms $C_T\Delta_{\rm NN}$, $C_T\Delta_{\rm OO}$ (with the above discussed result $\Delta_{\rm NN} = \Delta_{\rm OO} = -\pi/48$), and $C_T\Delta_{\rm NO}$ (with $\Delta_{\rm NO} = \pi/24$, as shown in the last section). Therefore, the last term in Eq. (28) embodies as special cases dGF amplitudes (7) for standard (E,O) BCs in Eq. (6) [8,14,32]. The surface exponent $x_\varepsilon^{(s)} = d = 2$ (well established for (O,E,SB) surface universality classes [47]) associated with the third term in Eq. (28) corresponds at the same time to the scaling dimension of the stress-tensor component perpendicular to the surface $T_{\perp\perp}(\vec{r}_{||}, z\to 0)$.

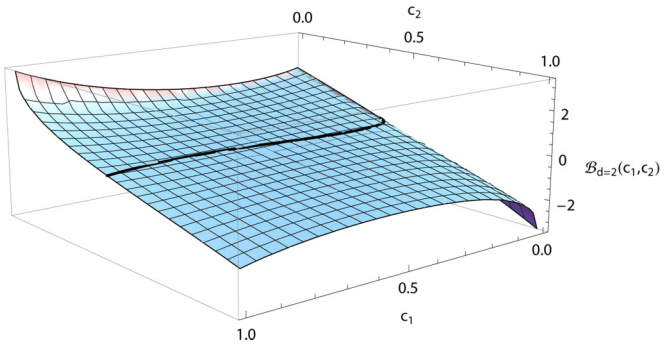

FIG. 4. (Color online) The universal dGF amplitude $\mathcal{B}_{d=2}(c_1,c_2) = \int_0^\infty \mathcal{D}(c_1,t)\Delta(c_1,c_2,t)dt$, $[c_i := y_i/(1+y_i)]$, $y_i := (Dh_i)^2 L, (i = 1,2)$ associated with the distant-wall correction term x^2 of Eq. (28) in dimension $d = 2$, featuring the reversal of its sign from positive values to negative ones. The bold line in the figure delimits domains of opposite signs of the dGF amplitude. The picture does not encompass the line $c_1 = 1$ as a separate case.

Previous studies, as explained above, based on the conformal invariance theory established that the stress-tensor component $T_{\perp\perp}(\vec{r}_{||}, z\to 0)$ must be contained in the short-distance expansion for (O,E,SB) surface universality classes and therefore it completely determines [16,46] the structure of the distant-wall correction via Eqs. (23)–(26). In this sense Eqs. (28), (30), and (22) with their structure unequivocally imply that the stress-tensor component perpendicular to the surface $T_{\perp\perp}(\vec{r}_{||}, z\to 0)$ preserve for the current variable symmetry-breaking BCs its earlier role in the short-distance expansion within the second-wall correction $\tilde{B}_d(y_1,y_2)x^d$. The *generalized* dGF amplitude, as it follows from current calculations (28), is defined as an integral over the product of two amplitude functions:

$$\tilde{B}_d(y_1,y_2) = (d-1)\int_0^\infty \tilde{\mathcal{D}}_d(y_1,t)\Delta_d^{(k)}(y_1,y_2,t)dt. \qquad (31)$$

This is a striking result since conformal invariance symmetry is presently *broken*.

The issue of *hyperuniversality* of the quantity C_T for (O,E) surface universality classes [16] drew significant attention in the past. It was found out that, although C_T *is* hyperuniversal in $d = 2$ (due to the property of the stress-tensor correlation function $\langle T_{\perp\perp}T_{\perp\perp}\rangle/x_\varepsilon^{(s)}$), this property does not exist in higher dimensions $d > 2$ (see Ref. [48] and references therein). Contrary to the case of standard surface universality classes, the amplitude $\tilde{\mathcal{D}}(y_1,t)$ defined by Eqs. (28) and (30) in $d = 2$ as a natural analog of the former C_T (7), explicitly depending on the surface field variable y_1, is *not* hyperuniversal even in the dimension $d = 2$ for the current BCs.

The first distant-wall correction $x\mathcal{C}(y_1,y_2)$ of Eq. (28) as a leading asymptotic contribution to EDPs generalizes Eqs. (23) and (27) ($\Phi = 0$ in $d = 2$) for variable BCs. In higher dimensions ($d > 2$) it would attain the form $x^{d-1-\Phi/\nu}\mathcal{C}_d(y_1,y_2)$ and would comprise a (SB) fixed point as a borderline case.

IV. ISING STRIPS: ADJUSTABLE SURFACE FIELDS AND GRAIN BOUNDARY

A. Energy density profiles

We proceed with the previous analysis, making our consideration more involved by introducing an internal defect "plane" as a model of the GB. I examine important aspects when this perturbation, so often encountered in real physical systems, affects the behavior of critical confined Ising systems. I modify in this section previously assumed geometry by placing the GB now at the coordinate origin $z = 0$, while surface planes are at points $z = -L/2$ (characterized by surface variable y_1) and $z = L/2$ (specified by another independent surface field variable y_2).

First, I deal with the analysis of EDPs for arbitrary *finite* values of field variables $0 < y_i < \infty$ $(i = 1,2)$, and GB's strength g. I highlight physically important limits $g = \pm\infty$. Second, I show that in the case of standard BCs (NN), (OO), and (NO,) the general solutions for EDPs $\varepsilon(x,y_1,y_2,g)$ acquire closed analytic forms, which, among other relevant information, provide new symmetry properties between them which are also relevant to Casimir effect.

The general solution to Euler-Lagrange equation of functional (8) at the bulk criticality is modified with respect to Eq. (10) in the present situation,

$$\varepsilon_q(z) = \begin{cases} \operatorname{csch}(Lq)\left\{\varepsilon_q^{(0)}\sinh[q(L-2z)] + \varepsilon_q^{(2)}\sinh(2qz)\right\}, & 0 < z < L/2, \\ -\operatorname{csch}(Lq)\left\{\varepsilon_q^{(1)}\sinh(2qz) - \varepsilon_q^{(0)}\sinh[q(L+2z)]\right\}, & -L/2 < z < 0, \end{cases} \tag{32}$$

where $\varepsilon_q^{(1)} = \varepsilon_q(z=-L/2)$ and $\varepsilon_q^{(2)} = \varepsilon_q(z=L/2)$ are boundary surface energy modes, while $\varepsilon_q^{(0)} = \varepsilon_q(z=0)$ is another mode associated with the GB. Then I calculate $\varepsilon_q^{(i)}$ $(i=0,1,2)$ from boundary conditions given by Eq. (11) (modified with respect to new positions of boundary surfaces) and (17). Employing earlier variables $x := z/L$, $t := qL$, and $y_i = D^2h_i^2L$ $(i=1,2)$, after substituting solutions $\varepsilon_q^{(i)}$ $(i=0,1,2)$ into Eq. (32), I derive the following form of energy density modes:

$$\varepsilon_q(z) = \begin{cases} \frac{\cosh(g)[\cosh(2tx)(t^2-y_1y_2)+t(y_1-y_2)\sinh(2tx)]+\sinh(g)\{\cosh[t(1-2x)](t^2+y_1y_2)+t(y_1+y_2)\sinh[t(1-2x)]\}}{\sinh(g)(t^2-y_1y_2)+\cosh(g)[\cosh(t)(t^2+y_1y_2)+t\sinh(t)(y_1+y_2)]}, & 0 < x < \frac{1}{2}, \\ \frac{\cosh(g)\cosh(2tx)(t^2-y_1y_2)+\sinh(g)\cosh[t(2x+1)](t^2+y_1y_2)+t\{\cosh(g)(y_1-y_2)\sinh(2tx)+\sinh(g)(y_1+y_2)\sinh[t(2x+1)]\}}{\sinh(g)(t^2-y_1y_2)+\cosh(g)[\cosh(t)(t^2+y_1y_2)+t\sinh(t)(y_1+y_2)]}, & -\frac{1}{2} < x < 0. \end{cases} \tag{33}$$

EDPs $\varepsilon(x,y_1,y_2,g)$ follow from the integration (12) of the last solution (33). I present curves of $\varepsilon(x,y_1,y_2,g)$ in Fig. 5 for a couple of arbitrarily chosen values of surface field variables $y_1 = 8$ and $y_2 = 17$ and a few positive and negative values of the GB field g, $g = \pm 1, \pm 0.01$.

Figure 6 also examines EDPs for *higher* arbitrarily fixed values of surface variables $y_1 = 20$ and $y_2 = 60$ and various values of the field g, $g = \pm 2, \pm 0.01$. We should recall that the GB field g controls within the present continuum model the strength K_0 of a bonding between spins in the ladder type of the GB in the lattice model formulation via the exponential law [13] $\exp(-g) \sim K_0$. Thus, values of $g = \pm 2, \pm 1$, used in Figs. 5 and 6 already prompt noticeable strengthening $(g < 0)$ or weakening $(g > 0)$ of the bond K_0 between surface spins. The smaller values of $g = \pm 0.01$ in Figs. 5 and 6 are culled to refer to the *linear regime* $g \ll 1$ that may draw separate attention [13] within the overall analysis, as I demonstrate later in this work.

All profiles $\varepsilon(x,y_1,y_2,g)$ in Figs. 5 and 6 are nonmonotonic and display minima near boundary surfaces for finite nonzero values of surface fields $0 < |h_i| < \infty$. We can notice that the GB greatly affects EDPs not only in the vicinity of the GB at $z = 0$ but throughout the film. This influence, as clearly seen from Fig. 5, reflects also in amplitudes of profiles' minima near boundary walls. For example, the higher are the *positive* values of g, such as $g = +1$ in Fig. 5(a), the lesser are the amplitudes of minima in comparison with the case of Fig. 5(c) derived for the lower value of the field $g = +0.01$. We see the signature of the GB for higher and lower *negative* values of the field g in Figs. 5(b) and 5(d), where larger negative g makes minima generally deeper. EDPs for *larger* surface field variables $y_1 = 20$, $y_2 = 60$ in Fig. 6 behave qualitatively similarly to those in Fig. 5, undergoing comprehensive changes due to the GB, except that their amplitudes are noticeably more stable with respect to the alteration of the GB strength g.

We additionally explain the behavior of EDPs in Figs. 5 and 6 with close insight into the role of the GB. Taking limit $L \to \infty$ in Eq. (33), one readily obtains from Eq. (12) the semi-infinite profile perturbed by a single GB:

$$\varepsilon(z,g) = \frac{\tanh(g)}{4\pi|z|}, \quad z \to \pm 0. \tag{34}$$

The last equation is exact in $d = 2$ at the bulk critical point T_c, as shown earlier by the conformal invariance theory [49], while it is a leading asymptotic contribution near the GB away

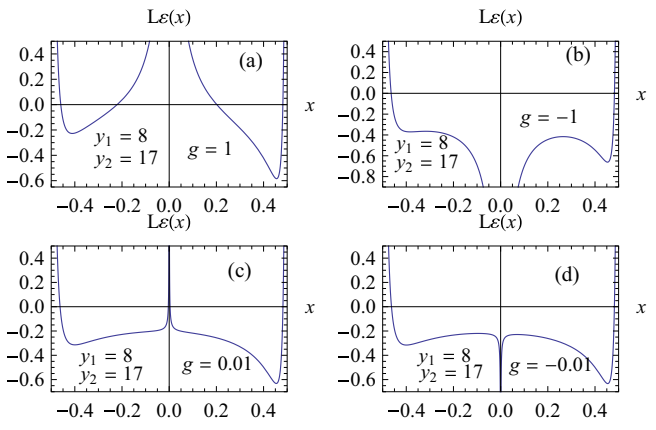

FIG. 5. (Color online) Plots of EDPs for arbitrary surface field variables $y_1 = 8$, $y_2 = 17$, calculated according to solution (33) and Eq. (12) for a pair of positive and negative values of the GB field g: (a) $g = 1$, (b) $g = -1$, (c) $g = +0.01$, (d) $g = -0.01$.

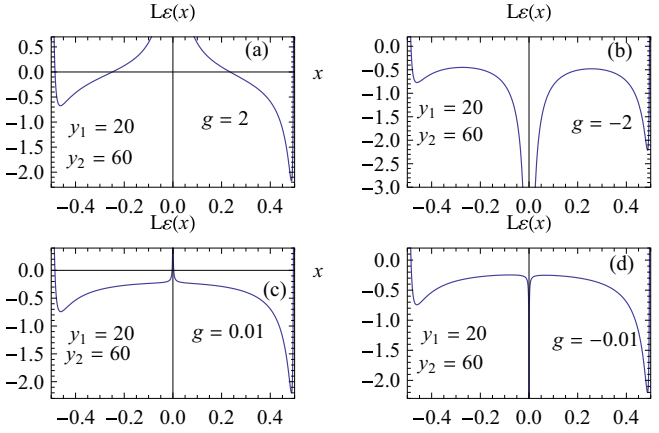

FIG. 6. (Color online) Plots of EDPs for a pair of larger arbitrary surface fields variables $y_1 = 20$, $y_2 = 60$, calculated according to the solution (33) and Eq. (12) for a pair of positive and negative values of the GB strength g: (a) $g = 2$, (b) $g = -2$, (c) $g = +0.01$, (d) $g = -0.01$.

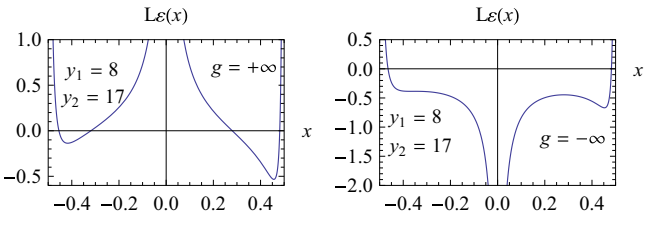

FIG. 7. (Color online) Plots of EDPs for a pair of arbitrary surface field variables $y_1 = 8$, $y_2 = 17$, calculated according to the solution (35) and Eq. (36) for limiting values of the GB strength g: (a) $g = +\infty$; (b) $g = -\infty$. EDPs are more positive and minima are shallower with the larger positive g.

from the critical point [13] $T \neq T_c$, so that when $g \to +\infty$, $K_0 \to 0$ and surface spins on the GB are completely free. Indeed, to corroborate quantitatively such reasoning we may use Eq. (20). In the limit when $z \to 0$, $y_1 \to 0$, referring to the (O) surface universality class, it follows from (20) that $\varepsilon_{\infty/2}(z,h_1) \to \frac{1}{4\pi z}$, in concordance with the limit $g \to +\infty$ of Eq. (34). On the other hand, when $g \to -\infty$, then $K_0 \to \infty$, implying that the surface spins on the GB are completely frozen, which is equivalent to the (N) BC. This is again validated by Eq. (20), from where it follows for $z \to 0$ and $y_1 \to +\infty$ for the (N) BC that $\varepsilon_{\infty/2}(z,h_1) \to -\frac{1}{4\pi z}$, in agreement with the limit $g \to -\infty$ of Eq. (34). This identification of limits $g \to \pm\infty$ with (O) and (N) BCs was shown as appropriate also in the off-critical regime [13], when fields h_1 and t became irrelevant at short wavelengths.

The interpretation of profiles in Figs. 5 and 6 and subsequently in Figs. 7 and 8 is clear and in accord with Ref. [13]: When $g > 0$, in particular $g \to +\infty$, the disordering effect of bonds in the original ladder GB of the lattice model increases the energy, making EDPs more positive. On the contrary, for $g < 0$, and especially $g \to -\infty$, large-scale fluctuations are abolished by the ordering effect of the GB's surface, making profiles negative.

We also consider limits $g \to \pm\infty$ within EDPs that follow from Eq. (33). This sheds additional light onto the above discussion on (O) and (E) BCs derived from limits $g \to +\infty$ and $g \to -\infty$ of Eq. (34), respectively. Equation (33) in the limit $g \to +\infty$ becomes

$$\varepsilon_q(x,y_1,y_2,g \to +\infty) = \begin{cases} \frac{t\cosh[t(1+4x)/2]+y_1\sinh[t(1+4x)/2]}{t\cosh(t/2)+y1\sinh(t/2)}, & -\frac{1}{2} < x < 0, \\ \frac{t\cosh[t(1-4x)/2]+y_2\sinh[t(1-4x)/2]}{t\cosh(t/2)+y1\sinh(t/2)}, & 0 < x < \frac{1}{2}, \end{cases} \quad (35)$$

while the same Eq. (33) in the limit $g \to -\infty$ transforms into

$$\varepsilon_q(x,y_1,y_2,g \to -\infty) = \begin{cases} -\frac{y_1\cosh[t(1/2+2x)]+t\sinh[t(1/2+2x)]}{y_1\cosh(t/2)+t\sinh(t/2)}, & -\frac{1}{2} < x < 0, \\ -\frac{y_2\cosh[t(1/2-2x)]+t\sinh[t(1/2-2x)]}{y_2\cosh(t/2)+t\sinh(t/2)}, & 0 < x < \frac{1}{2}. \end{cases} \quad (36)$$

Then, after integrating Eqs. (35) and (36) according to Eq. (12) I present EDPs $\varepsilon(x,y_1,y_2,g\to+\infty)$ and $\varepsilon(x,y_1,y_2,g\to-\infty)$

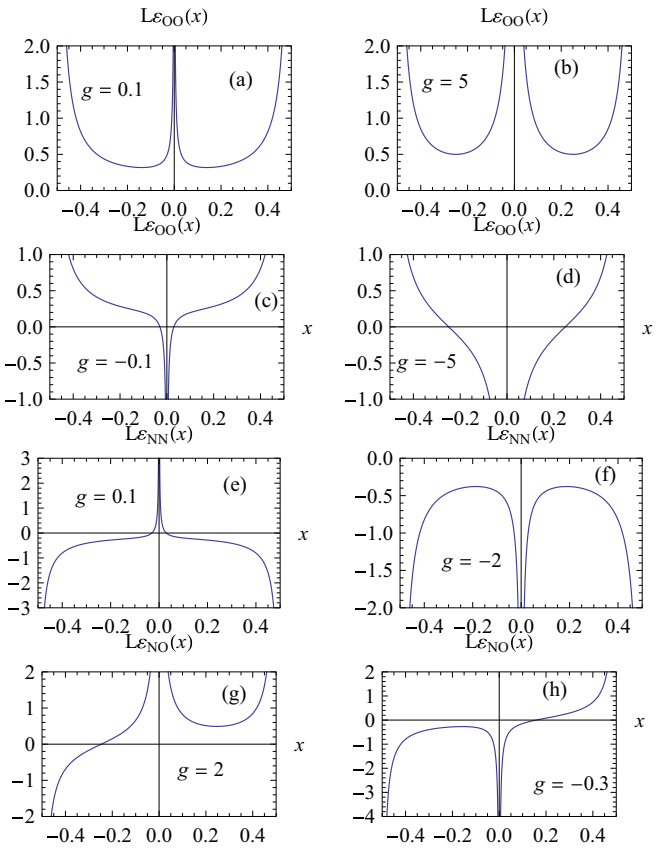

FIG. 8. (Color online) Plots of EDPs when both confining surfaces belong to standard surface universality classes (N) and (O) for several arbitrary positive and negative values of the GB strength parameter g: (a) (OO) BC with $g = +0.1$, (b) (OO) BC, $g = +5$, (c) (OO) BC, $g = -0.1$, (d) (OO) BC, $g = -5$, (e) (NN) BC, $g = +0.1$, (f) (NN) BC, $g = -2$, (g) (NO) BC, $g = +2$, (h) (NO) BC, $g = -0.3$. Plots for (NN) and (OO) BCs are based on solutions (A1) and (A2) of the Appendix, respectively. The curves for (NO) BC were derived by Eq. (42).

in Figs. 7(a) and 7(b), respectively. Qualitatively similar commentary connected with Figs. 5 and 6 applies to the behavior of EDPs in Figs. 7(a) and 7(b). Yet, present situations $g = \pm\infty$ stand out for a new feature. Borderline cases $g \to \pm\infty$ cause the original film to split into two independent halves (each of width $L/2$) defined on the subintervals $x \in [-1/2,0]$ and $x \in [0,1/2]$. This may be perceived from Eqs. (35) and (36), where branches of the solutions on the intervals $x \in [-1/2,0]$ and $x \in [0,1/2]$ completely lack information on the BC of the opposite wall, that is, y_2 and y_1, respectively. Each part of the solution apparently contains either the surface variable y_1 (left half of the strip) or y_2 (right half of the film). Then the intuitively appealing interpretation that the second BC in corresponding subfilms corresponds either to the (N) BC when $g \to -\infty$ or to the (O) BC when $g \to +\infty$ may be confirmed analyzing the general solution (19) rescaled to width $L/2$ and translated for distance $-L/2$ when necessary. We take at the same time either limits $y_i \to \infty$ or $y_i \to 0$ $(i = 1,2)$ and thus we map (19) onto Eqs. (35) and (36), respectively.

We gain useful insights from the general solution (33) into behavior of critical Ising strips with the internal defect plane of arbitrary strength g for standard BCs (NN), (OO), and (NO) in $d = 2$. Taking limits $y_1 \to \infty$, $y_2 \to \infty$, which correspond to the (NN) BC, we obtain for energy density modes

$$\varepsilon_q^{\mathrm{NN}}(x,g) = \begin{cases} -\frac{\cosh(2tx)\cosh(g)+\sinh(g)\cosh[t(1+2x)]}{\cosh(g)\cosh(t)-\sinh(g)}, & -\frac{1}{2} < x < 0, \\ -\frac{\cosh(g-2tx)+\cosh(g+2tx)-2\cosh[t(1-2x)]\sinh(g)}{2\cosh(g)\cosh(t)-2\sinh(g)}, & 0 < x < \frac{1}{2}. \end{cases} \tag{37}$$

Integration of energy modes (37) with the help of (12) may be performed analytically providing us with a closed form for EDPs $\varepsilon_{\mathrm{NN}}(x,g)$. As this solution is lengthier, I give it in the Appendix by Eq. (A1). It turns out that knowledge of $\varepsilon_{\mathrm{NN}}(x,g)$ together with other results that follow will enable us to infer important symmetry features of EDPs for fixed-point (NN) and (OO) BCs with an internal GB.

Letting $y_1 \to 0$ and $y_2 \to 0$ in Eq. (33) correspond to (OO) BC:

$$\varepsilon_q^{\mathrm{OO}}(x,g) = \begin{cases} \frac{\cosh(g-2tx)+\cosh(g+2tx)+\cosh[t(1-2x)]\sinh(g)}{2[\cosh(g)\cosh(t)+\sinh(g)]}, & 0 < x < \frac{1}{2}, \\ \frac{\cosh(g-2tx)+\cosh(g+2tx)+2\cosh[t(1+2x)]\sinh(g)}{2[\cosh(g)\cosh(t)+\sinh(g)]}, & -\frac{1}{2} < x < 0. \end{cases} \tag{38}$$

Closed analytic form for EDPs $\varepsilon_{\mathrm{OO}}(x,g)$, given in the Appendix by Eq. (A2), follows from integrating the last equation according to Eq. (12).

Profiles $\varepsilon_{\mathrm{NN}}(x,g)$ and $\varepsilon_{\mathrm{OO}}(x,g)$ given by Fig. 8 obviously show the absence of their nonmonotonic behavior near boundary surfaces. This is expected due to the fact that the other characteristic length l_1 (3), besides the film width L, which is responsible for nonmonotonicity properties of order-parameter profiles, becomes irrelevant for either $y_i \to \infty$ or $y_i \to 0$ $(i = 1,2)$. While profiles $\varepsilon_{\mathrm{NN}}(x,g)$ diverge always downward near surfaces, profiles $\varepsilon_{\mathrm{OO}}(x,g)$ tend to $+\infty$ just as in the former case of Fig. 1. Both types of profiles $\varepsilon_{\mathrm{NN}}(x,g)$ and $\varepsilon_{\mathrm{OO}}(x,g)$ behave near GB asymptotically in accord with Eq. (34).

We generalize the previous trait of EDPs without GB (21) for the Ising strip with internal defect of strength g as

$$\varepsilon_{\mathrm{OO}}(x,g) = -\varepsilon_{\mathrm{NN}}(x,-g), \tag{39}$$

which is consequent to Eqs. (A1) and (A2). Indeed, the last feature is also evident in Figs. 8(c) and 8(e). Apparently due to the inherent symmetry of (NN) and (OO) BCs it also holds,

$$\varepsilon_{\mathrm{OO}}(x,g) = -\varepsilon_{\mathrm{NN}}(-x,-g), \tag{40}$$

which ensues from Eqs. (A1) and (A2) as well.

We complete the current exposition of EDPs for standard surface universality classes with (NO) BC. Taking limits $y_1 \to \infty$ and $y_2 \to 0$ in Eq. (33) yields

$$\varepsilon_q^{\mathrm{NO}}(x,g) = \begin{cases} \mathrm{csch}(t)\{\sinh(2tx) - \sinh[t(1-2x)]\tanh(g)\}, & 0 < x < \frac{1}{2}, \\ \mathrm{csch(t)}\{\sinh(2tx) + \sinh[t(1+2x)]\tanh(g)\}, & -\frac{1}{2} < x < 0. \end{cases} \tag{41}$$

An integration of the last expression in Eq. (12) provides an analytic solution for EDPs $\varepsilon_{\mathrm{NO}}(x,g)$:

$$\varepsilon_{\mathrm{NO}}(x,g) = \begin{cases} \frac{1}{4L}[\tan(\pi x) + \cot(\pi x)\tanh(g)], & 0 < x < \frac{1}{2}, \\ \frac{1}{4L}[\tan(\pi x) - \cot(\pi x)\tanh(g)], & -\frac{1}{2} < x < 0. \end{cases} \tag{42}$$

Plots of profiles $\varepsilon_{\mathrm{NO}}(x,g)$ according to the solution (42) are given by Figs. 8(g) and 8(h). Due to different surface universality classes: (N) at $z = L/2$ and (O) at $z = L/2$, profiles diverge near boundaries to $-\infty$ and $+\infty$, respectively. Of course, near the GB at $z = 0$, $\varepsilon_{\mathrm{NO}}(x,g)$ abides by Eq. (34) continuously changing with the field g. Equation (42) implies the following parity features of EDPs $\varepsilon_{\mathrm{NO}}(x,g)$:

$$\varepsilon_{\mathrm{NO}}(-x,g) = -\varepsilon_{\mathrm{NO}}(x,g), \tag{43a}$$

$$\varepsilon_{\mathrm{NO}}(x,-g) = \varepsilon_{\mathrm{NO}}(-x,g). \tag{43b}$$

B. Modified Casimir amplitudes

I am interested here how the Casimir force at T_c behaves when in addition to surface fields, considered in Sec. III B, the GB is present in the system. I examine first CAs $\Delta(y_1,y_2,g)$ for assigned positive $g > 0$ and negative $g < 0$ discrete values of the GB strengths g. Within the scope of this discussion, depending on the magnitude of the field $|g|$, I comment on the similarity and difference of present CAs with respect to the case when the GB is absent from the system as elaborated in Sec. III B. I also attend to qualitative symmetry that is discerned between CAs $\Delta(y_1,y_2,g)$ and $\Delta(y_1,y_2,-g)$, which attains a more pronounced, although still approximate, form for infinite values of the field g, $g \to \pm\infty$. In order to shed more light onto the structure of CAs $\Delta(y_1,y_2,g)$ as well as onto a separate impact of the GB onto their behavior, I also examine $\Delta(y_1,y_2,g)$ as a continuous function of the field parameter g in cases of *symmetric* $(h_1 = h_2)$ and *asymmetric* $(h_1 \neq h_2)$ BCs. This analysis enables us to discuss once again the approximate symmetry between CAs $\Delta(y_1,y_2,g)$ and $\Delta(y_1,y_2,-g)$ for larger values of g especially for $g \to \pm\infty$ when the field g controls CAs dominantly in comparison with surface fields h_i $(i = 1,2)$. Additionally, it turns out that CAs manifest interesting behavior also for *small* values of the GB field g, $g \ll 1$, that I highlight within the current analysis.

We base the present analysis on the formula (15) of Sec. III B and the general solution (33) of Sec. IV A, which takes into account the influence of the GB field of strength g in the Ising strip. From Eqs. (15) and (33) we determine the following generalization of Eq. (22) for CA:

$$\Delta(y_1,y_2,g)=\int_0^\infty \Delta^{(k)}(y_1,y_2,t,g)dt, \tag{44a}$$

$$\Delta^{(k)}(y_1,y_2,t,g)=(1-\delta_{g,0}/2)\frac{\exp(-t)t[(t-y_1)(t-y_2)\cosh(g)+\exp(t)(t^2-y_1y_2)\sinh(g)]}{\pi\{(t^2-y_1y_2)\sinh(g)+\cosh(g)[(t^2+y_1y_2)\cosh(t)+t(y_1+y_2)\sinh(t)]\}}, \tag{44b}$$

where $\delta_{g,0}$ is Kronecker δ symbol and variable $t:=qL$ and y_i $(i=1,2)$ are surface field variables. Before examining the formula (44) it is useful for subsequent considerations to derive separately CAs in the pronounced limits $g\to\pm\infty$ of Eq. (44):

$$\Delta^{(k)}(y_1,y_2,t,g\to+\infty)=\frac{t[(t-y_1)(t-y_2)+(t^2-y_1y_2)\cosh(t)+(t^2-y_1y_2)\sinh(t)]}{2\pi[t\cosh(t/2)+y_1\sinh(t/2)][t\cosh(t/2)+y_2\sinh(t/2)][\cosh(t)+\sinh(t)]}, \tag{45a}$$

$$\Delta^{(k)}(y_1,y_2,t,g\to-\infty)=\frac{t\{t(y_1+y_2)+t^2[-1+\cosh(t)+\sinh(t)]-y_1y_2[1+\cosh(t)+\sinh(t)]\}}{2\pi[y_1\cosh(t/2)+t\sinh(t/2)][y_2\cosh(t/2)+t\sinh(t/2)][\cosh(t)+\sinh(t)]}. \tag{45b}$$

We first plot manifolds of CAs $\Delta(y_1,y_2,g)$ in the space spanned by redefined surface field variables $c_i=\frac{y_i}{1+y_i}$, $(i=1,2)$ for several characteristic positive and negative values of the GB field g, based on Eq. (44). Figures 9 and 10 present CAs $\Delta(c_1,c_2,g)$ for *positive* and *negative* values of g, respectively running from $|g|=+1$ up to the very small value of $|g|=+0.01$. We notice that CAs $\Delta(c_1,c_2,g)$ for *larger* $|g|$ [cf. Figs. 9(a) and 10(a) for $g=+1$ and $g=-1$, respectively] are very much different from the one in Fig. 2 of Sec. III B realized in the absence of the GB, that is, $g=0$. First, they are characterized only by a single line of zeros $\Delta(c_1^\star,c_2^\star,g)=0$ separating positive $\Delta(c_1,c_2,g)>0$ from negative values $\Delta(c_1,c_2,g)<0$ of CA instead of earlier two separate lines in Fig. 2 disconnecting areas of positive values

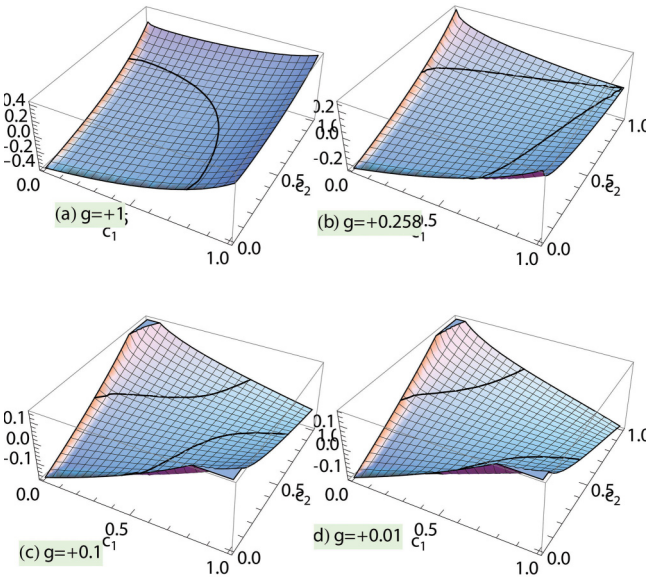

FIG. 9. (Color online) Plots of CAs (44) $\Delta(c_1,c_2,g)$ in the space of reduced surface fields variables $c_i=\frac{y_i}{1+y_i}$, $(i=1,2)$ for several positive GB strengths g: (a) $g=+1$, (b) $g=+0.258$ is near the borderline case $g_1^\star\simeq 0.246$ between cases (a) and (c), when the earlier single connected area of positive $\Delta>0$ transforms into two disconnected wings of positive values of CAs, delimited in the panels by bold lines; (c) $g=+0.1$ and (d) $g=+0.001$. Symmetry of the manifold $\Delta(c_1,c_2,g>0)$ with respect to the axis $c_1=c_2$ gradually sets in for smaller values of g, as shown in cases (c) and (d). Areas of the repulsive $\Delta(c_1,c_2,g)>0$ and the attractive $\Delta(c_1,c_2,g)<0$ Casimir force are marked off by bold lines in all panels. Extreme values $\Delta_{\max}$ and $\Delta_{\min}$ may be roughly ten times larger than the corresponding ones in the case without the GB, as in Fig. 2.

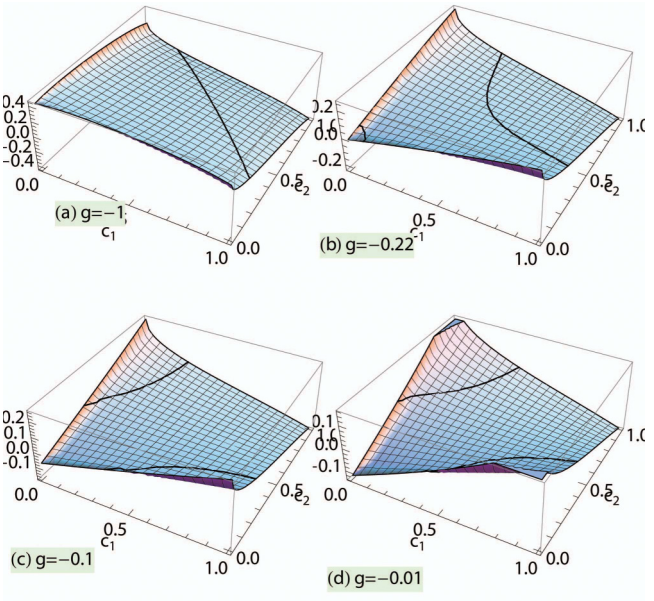

FIG. 10. (Color online) CAs (44) $\Delta(c_1,c_2,g)$ in the space of reduced surface fields variables $c_i=\frac{y_i}{1+y_i}$, $(i=1,2)$ for several negative GB strengths g: (a) $g=-1$, (b) $g=-0.22$, close to the borderline value $g_2^\star\simeq-0.235$, presents the onset of the second wing of positive CAS $\Delta(c_1,c_2,g)>0$ situated at the corner $(c_1,c_2)=(0,0)$; (c) $g=-0.1$, (d) $g=-0.01$. CAs $\Delta(c_1,c_2,g<0)$ are symmetric with respect to the axis $c_1=c_2$ for smaller values of the GB field $|g|$, as evident in cases (c) and (d). Areas of repulsive $\Delta(c_1,c_2,g)>0$ and attractive $\Delta(c_1,c_2,g)<0$ Casimir forces are marked off by bold lines in all panels. Extreme values $\Delta_{\max}$ and $\Delta_{\min}$ may be roughly ten times larger than the corresponding ones when the GB is missing as in Fig. 2.

$\Delta(c_1,c_2,g) > 0$ symmetrically placed around the domain of negative values $\Delta(c_1,c_2,g) < 0$. Apart from this, it is also noticeable from Figs. 9(a) and 10(a) as well as from other calculations that extreme positive $\Delta_{\max}(c_1',c_2',g)$ and negative values $\Delta_{\min}(c_1'',c_2'',g)$ are roughly more than ten times larger than in Fig. 2 as a manifest consequence of the GB's influence on the Ising strip. We may conclude that Casimir force may significantly be magnified toward positive or negative values for certain domains of surface variables (c_1,c_2) combined with a conspicuous effect of the GB.

As the GB strength $|g|$ grows less, evolution of Casimir manifold resembles previously shown Fig. 2 as we see in Figs. 9(c), 9(d), 10(c), and 10(d) for positive $g > 0$ and negative $g < 0$, respectively. However, even in such cases the interval $[\Delta_{\max}(g) > 0, \Delta_{\min}(g) < 0]$ of possible values of CA, although diminishing with a decrease of the field g, is still definitely larger than in Fig. 2. Figures 9(d) and 10(d) correspond to the *linear* regime with respect to the parameter g. The similarity of CAs $\Delta(c_1,c_2,g)$ with the case of $\Delta(c_1,c_2)$ free of GB in Fig. 2 holds within an almost symmetrical interval $g \in (g_2^\star \simeq -0.235, g_1^\star \simeq 0.246)$. This also implies the mutual resemblance of surfaces $\Delta(y_1,y_2,g > 0)$ [Figs. 9(c) and 9(d)] and $\Delta(y_1,y_2,g < 0)$ [Figs. 10(c) and 10(d)] in the linear regime of g. To reiterate, outside of this interval for $g \in (g_1^\star, +\infty)$ and $g \in (-\infty, g_2^\star)$ we have qualitatively different crossover behavior of $\Delta(c_1,c_2,g)$ from the unperturbed case $g = 0$ in Fig. 2, distinguished by single connected areas of positive and negative values. Figures 9(b) and 10(b) present CAs near borderline values of $g_1^\star$ and $g_2^\star$, respectively, and therefore they describe a transitory regime from one [cf. Figs. 9(a) and 10(a)] to another [cf. Figs. 9(c), 9(d), 10(c), and 10(d)] mode of their behavior.

We notice that structure of CA manifold $\Delta(c_1,c_2, g \to -\infty)$, presented by contour plots in Fig. 11(a), is *near symmetric* to $\Delta(c_1,c_2,g \to +\infty)$ in Fig. 11(b) with respect to the axis $c_1 + c_2 = 1$. This is especially apparent for positive contours. If the symmetry were exact, the axis $c_1 + c_2 = 1$ would be an intersection line of the two surfaces $\Delta(c_1,c_2,g \to -\infty)$ and $\Delta(c_1,c_2,g \to +\infty)$. Figure 12 shows

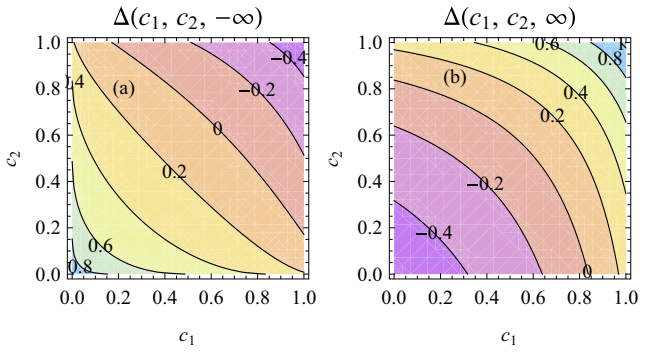

FIG. 11. (Color online) Contour plots of CAs $\Delta(c_1,c_2,g)$ for limiting cases (a) $g = -\infty$ and (b) $g = +\infty$, calculated by Eq. (45). Pictures present a qualitatively symmetric relationship of CAs in the above cases with respect to the axis $c_1 + c_2 = 1$. In particular, positive contours of $\Delta(c_1,c_2,g = -\infty)$ and $\Delta(c_1,c_2,g = +\infty)$ are in closer symmetric relation regarding both their positions and curvatures.

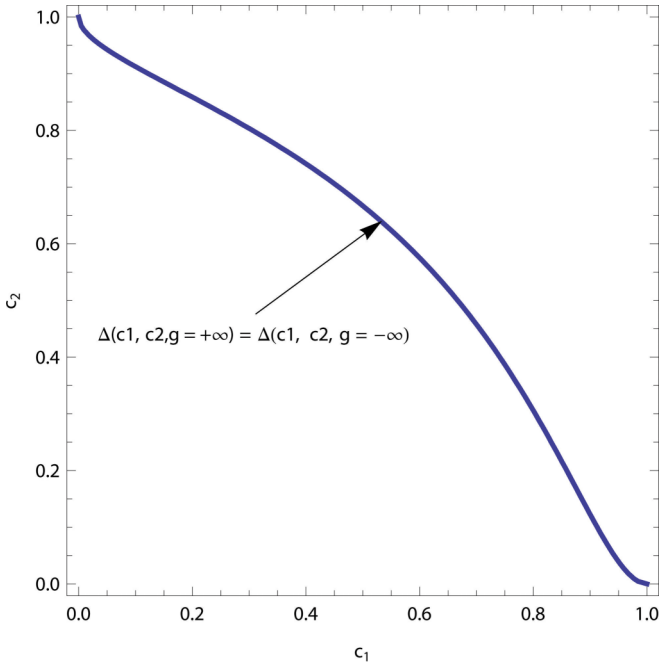

FIG. 12. (Color online) The line of intersection of CAs $\Delta(c_1,c_2,g = -\infty)$ and $\Delta(c_1,c_2,g = +\infty)$. The picture illustrates to what extent it deviates from the axis $c_1 + c_2 = 1$, as a part of the discussion on the symmetry between CAs $\Delta(c_1,c_2,g = -\infty)$ and $\Delta(c_1,c_2,g = +\infty)$.

the degree of deviation of the real line of intersection of CAs $\Delta(c_1,c_2,g \to -\infty) = \Delta(c_1,c_2,g \to +\infty)$ from the axis $c_1 + c_2 = 1$. The qualitatively symmetric relationship between CAs for $g \to \pm\infty$ with respect to the line $c_1 + c_2 = 1$ is related multifariously to very different role of the GB in these limits. The larger positive $g > 0$ affects the GB, making it eventually closer to the (O) surface universality class as argued in Sec. IV A. On the contrary, larger negative $g < 0$ accomplishes the GB's resemblance with the (N) BC. Then we see that borderline points $(c_1,c_2) = (0,0)$ and $(c_1,c_2) = (1,1)$ in fact influence affirmatively the above perceived symmetry between $\Delta(c_1,c_2,g \to -\infty)$ and $\Delta(c_1,c_2,g \to +\infty)$. Indeed, the point $(c_1,c_2) = (0,0)$ in Fig. 11(b), when $g \to +\infty$, corresponds to two subfilms with combined BCs (OO)(OO), resulting in the negative overall CA for the entire strip: $\Delta(c_1 = 0,c_2 = 0,g = +\infty)/L^2 \equiv \Delta_{(OO)(OO)}/L^2 = (-\pi/48)[1/(L/2)^2] + (-\pi/48)[1/(L/2)^2]$, that is, $\Delta(c_1 = 0, c_2 = 0, g = +\infty) = -\pi/6$. On the other hand, the point $(c_1,c_2) = (1,1)$ in Fig. 11(b) defines mixed (NO)(ON) BCs so that CA of the whole film is necessarily positive: $\Delta(c_1 = 1,c_2 = 1,g = +\infty)/L^2 \equiv \Delta_{(NO)(ON)}/L^2 = (\pi/24)[1/(L/2)^2] + (\pi/24)[1/(L/2)^2]$, that is, $\Delta(c_1 = 1,c_2 = 1,g = +\infty) = \pi/3$. Similarly, I identify CAs at the leading points $(c_1,c_2) = (0,0),(1,1)$ in Fig. 11(a). In this case the limit $g = -\infty$ corresponds to the GB of the type (N). I have mixed (ON)(NO) BCs at the point $(c_1,c_2) = (0,0)$ and therefore $\Delta(c_1 = 0,c_2 = 0,g = -\infty) = \pi/3$, which is exactly symmetric to $\Delta(c_1 = 1,c_2 = 1,g = +\infty)$ in Fig. 11(b). At the point $(c_1,c_2) = (1,1)$ in Fig. 11(a), arguing analogously, I obtain $\Delta(c_1 = 1,c_2 = 1,g = -\infty) = -\pi/6$ which is completely symmetric to $\Delta(c_1 = 0,c_2 = 0,g = +\infty)$ in Fig. 11(b).

This relationship among the CAs $\Delta(c_1,c_2,g\to+\infty)$ and $\Delta(c_1,c_2,g\to-\infty)$ at the prominent points $(c_1,c_2)=(0,0),(1,1)$ is also presented explicitly below in Fig. 15(b), which is a plane cut through space $[c_1,c_2,\Delta(c_1,c_2,g=\pm\infty)]$ along the diagonal $c_1=c_2$ of Figs. 11(a) and 11(b). The finite nonzero values of field variables $0<c_i<+1$ $(i=1,2)$ *away* from the borderline points $(c_1,c_2)=(0,0),(1,1)$ are in a more complex competition with GB fields $g=\pm\infty$, resulting in the overall deviation from the exact symmetry between CAs $\Delta(c_1,c_2,g\to+\infty)$ and $\Delta(c_1,c_2,g\to-\infty)$, as shown in Figs. 11(a) and 11(b).

The symmetriclike relation between $\Delta(c_1,c_2,g\to+\infty)$ and $\Delta(c_1,c_2,g\to-\infty)$ is worsened for *finite* values of $|g|$ due to a more intricate interplay between surface fields and the GB. Yet, symmetry between them is preserved for finite values of $|g|$ to a very limited extent, as noticeable, for example, in Figs. 9(a) and 10(a).

While Figs. 9, 10, and 11 explore CAs $\Delta(c_1,c_2,g)$ in the space spanned by surface field variables c_1 and c_2 for several arbitrary appropriate fixed positive and negative values of the GB field g, I now want to enquire about the same quantity defined by Eq. (44) as a function of the continuously changing variable g. Then, in order to produce three-dimensional manifolds of CA, I choose to present the two most characteristic cases: (i) *symmetric* BC, $h_1=h_2$ and (ii) *asymmetric* BC, $h_1\neq h_2$, when only surface variable c_2 is fixed arbitrarily, while c_1 varies in the whole range $c_1\in[0,1]$. Figure 13(a) presents the case (i) and Fig. 13(b) the case (ii) for arbitrarily fixed $c_2=0.8$. We see that $\Delta(c_1,c_2,g)$ is a smooth manifold in the whole interval of $g\neq0$. These pictures reveal that CAs for symmetric and asymmetric BCs are qualitatively alike: Manifolds $\Delta(c_1,c_2,g)$ are distinguished in both cases by two disconnected domains of positive values $\Delta(c_1,c_2,g)>0$ separated by a single valley of negative values $\Delta(c_1,c_2,g)<0$ between them. However, in case (ii) CA $\Delta(c_1,c_2,g)$ is not symmetric with respect to the line $g=0$, as evident from Fig. 13(b): The area of positive values $\Delta(c_1,c_2,g)>0$ near the corner $(c_1,g)=(0,-5)$ is notably smaller than the other one situated around the opposite corner $(c_1,g)=(1,5)$.

Here, when comparing Figs. 13(a) and 13(b) and observing their approximate resemblance, I really refer to global characteristics of manifolds, while their details may differ considerably, as I discuss. A closer look reveals that dissimilarities are rather severe between the two regimes near the line $g=0$, that is, in the linear domain of g. As the behavior of the Casimir force in the domain of small values of the GB field g is characterized by several interesting features, I first examine independently the linear domain $|g|\ll1$ for symmetric and antisymmetric BCs.

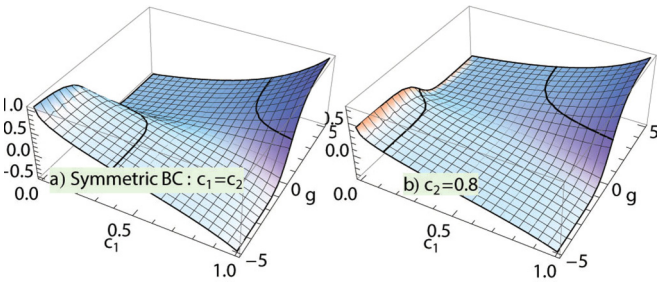

FIG. 13. (Color online) CAs (44) $\Delta(c_1,c_2,g)$ in the space of reduced surface field variable $c_1=\frac{y_1}{1+y_1}$ and the GB field parameter g for two characteristic cases of (a) *symmetric* BC, $h_1=h_2$, and (b) *asymmetric* BC, $h_1\neq h_2$, with c_2 fixed arbitrarily $c_2=0.8$. Areas of repulsive Casimir force $\Delta(c_1,c_2,g)>0$ are confined by bold lines from the complementary area of the attractive Casimir force $\Delta(c_1,c_2,g)<0$.

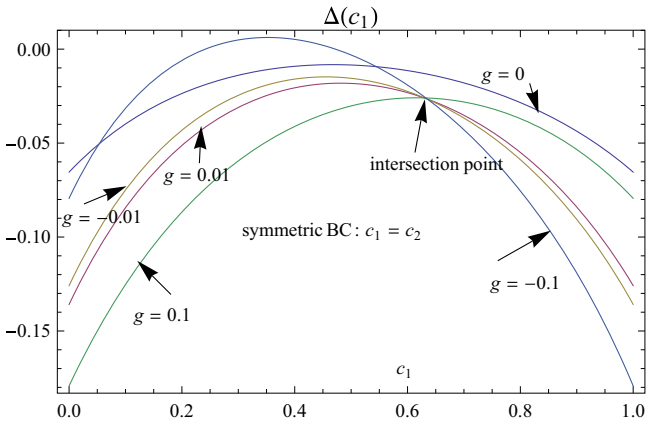

FIG. 14. (Color online) The CAs (44) $\Delta(c_1,g)$ for *symmetric* BC $h_1=h_2$ for several smaller positive and negative values of the GB field g: $g=\pm0.01,\pm0.1$ Also shown in the same picture is a limiting case without the GB: $g=0$. CAs $\Delta(c_1,g)$ are *always attractive* for symmetric BC, either without GB $(g=0)$ or for smaller values of the field $g\ll1$ that correspond to the *linear regime*. All curves in the above picture intersect in the common point $(c_1^\star,\Delta(c_1^\star,g\ll1))=(0.631,-0.0255)$.

Figure 13(a) shows CAs $\Delta(c_1,g)$, $c_1\in[0,1]$, for (i) symmetric BC $(c_1=c_2)$ in the linear regime of g for several casually fixed values of g: $g=\pm0.1,\pm0.01$. The same picture contains for comparison CA in the strip without the GB, $g=0$. We see that in the case when there is no GB the Casimir force for the *like* BC $(h_1=h_2)$ is *always attractive* for planar surfaces: $F_{\rm Cas}(g=0)<0$. This generalizes earlier conclusions that the Casimir force is attractive for [50] $(++)$ BCs in all dimensions [51–53]. The curve of $\Delta(c_1=c_2,g=0)$ appears as a kind of an envelope for curves $\Delta(c_1=c_2,g\ll1)$, as we can notice for $g=\pm0.01$ and even greater $g=+0.1$. We may also conclude from Fig. 14 that CAs $\Delta(c_1=c_2,g\ll1)$ retain the most distinctive feature of $\Delta(c_1=c_2,g=0)$ to be always negative; that is, $\Delta(c_1=c_2,g\ll1)<0$ on the whole interval $c_1\in[0,1]$, notwithstanding whether $g>0$ or $g<0$. This is an unexpected result given the high sensitivity of profiles to the sign of g as shown in Sec. IV A.

It is interesting to recognize in Fig. 14 the *nodal singular point* [54,55] for the family of curves $\Phi(c_1,\Delta,g\ll1)=0$, which is, of course, at the same time the *characteristic* point [56]. The unique point of intersection is determined by

$$(c_1^\star,\Delta(c_1^\star,g\ll1))=(0.631,-0.0255). \tag{46}$$

We also discern that the inequality $\Delta(c_1^\star,g\ll1)<\Delta(c_1^\star,g=0)$ always holds. The singular point $(c_1^\star,\Delta(c_1^\star,g\ll1))$, since it is unique for *all* CAs $\Delta(c_1,g\ll1)$ in the linear regime of g, may be credited with a more meaningful connotation as the universal feature of the confined Ising strip with the GB for

symmetric ($h_1 = h_2$) BC. Also, in Fig. 14 it is noteworthy that the Casimir force with linear perturbation $g \ll 1$ is always *more strongly attractive* than the one without the GB:

$$\Delta(c_1, g \ll 1) < \Delta(c_1, g = 0). \tag{47}$$

This becomes especially pronounced at end points, where both $\Delta(c_1 = 1, g \ll 1) \equiv \Delta_{\rm NN}(g \ll 1)$ and $\Delta(c_1{=}0, g \ll 1) \equiv \Delta_{\rm OO}(g \ll 1)$ are remarkably smaller than corresponding CAs without GB, $\Delta_{\rm NN} = \Delta_{\rm OO} = -\pi/48$, therefore implying that even small perturbation $g \ll 1$ always makes the attractive Casimir force stronger than the unperturbed one $g = 0$ and even more so toward end points of the curve $\Delta(c_1, g \ll 1)$, *irrespective of the sign of the GB field* g.

We now examine the linear regime of g in Fig. 13(b), which I have designated as the asymmetric case (ii). Plots of $\Delta(c_1, c_2 = 0.8, g)$ for the arbitrary value of $c_2 = 0.8$ and very small g, $g = \pm 0.05$, are given in Fig. 16(a). Curves $\Delta(c_1, c_2 = 0.8, g = +0.05)$ and $\Delta(c_1, c_2 = 0.8, g = -0.05)$ are very close to each other in the linear regime, yet completely different from the symmetric case (i) in Fig. 14: CAs may now acquire both positive (for $c_1 < \tilde{c}_1^{+} \simeq 0.398$ when $g = +0.05$ and $c_1 < \tilde{c}_1^{-} \simeq 0.399$ when $g = -0.05$) and negative values (for $c_1 > \tilde{c}_1^{+}$ or $c_1 > \tilde{c}_1^{-}$). It turns out that CAs $\Delta(c_1, c_2 = 0.8, g \ll 1)$ in the linear regime of g are also characterized by a nodal singular point,

$$(c_1^{\star}, \Delta(c_1^{\star}, c_2 = 0.8, g \ll 1)) = (0.405, -0.001), \tag{48}$$

the existence of which is analogous to Eq. (46) and Fig. 14.

We further delve into specific areas of the manifold in Fig. 13 by fixing g at *larger* values $g = \pm 0.5$ and borderline values $g = \pm\infty$. Curves $\Delta(c_1, g = \pm 0.5)$ and $\Delta(c_1, g = \pm\infty)$ for symmetric BC are given by Fig. 15. We now notice the tendency for curves $\Delta(c_1, g)$ and $\Delta(c_1, -g)$ to split entirely. From Fig. 15 it is apparent that for much of the interval of the variable c_1 it holds that $\Delta(c_1, g)\Delta(c_1, -g) < 0$; that is, CAs have opposite signs, except in narrow intervals around intersection points $c_1^{\star}$, $\Delta(c_1^{\star}, g) = \Delta(c_1^{\star}, -g)$. Indeed, results in Fig. 15(b) for $g = \pm\infty$ [which is cut out of Figs. 11(a) and 11(b) along the diagonals] support strongly the above perceived approximate symmetry between CAs $\Delta(c_1, c_2, g = +\infty)$ and $\Delta(c_1 = 0, c_2 = 0, g = -\infty)$ in Figs. 11 and 12. Earlier noticed exact symmetric relationships $\Delta(c_1 = 0, c_2 = 0, g = +\infty) = \Delta(c_1 = 1, c_2 = 1, g = -\infty) = -\pi/6$ and $\Delta(c_1 = 0, c_2 = 0, g = -\infty) = \Delta(c_1 = 1, c_2 = 1, g = +\infty) = -\pi/3$ are explicitly presented in Fig. 15(b) at the curves' end points $(c_1, c_2) = (0,0), (1,1)$. A qualitatively similar scenario is maintained for larger finite values of $\pm|g|$, as in Fig. 15(a) for $g = \pm 0.5$.

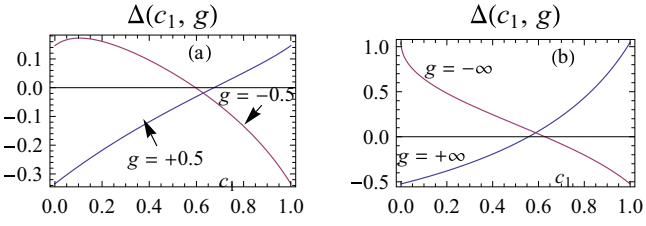

FIG. 15. (Color online) CAs (44) $\Delta(c_1, g)$ for *symmetric* BC $h_1 = h_2$ for *larger* positive and negative values of the GB field g: (a) $g = \pm 0.5$ and (b) $g = \pm\infty$. CAs are both attractive and repulsive for symmetric BC when field g attains larger values. CAs $\Delta(c_1, g)$ and $\Delta(c_1, -g)$ have a tendency to behave in the opposite manner for larger strengths g, that is, $\Delta(c_1, g)\Delta(c_1, -g) < 0$ for most of the interval of the variable c_1, except in narrow intervals around intersection points.

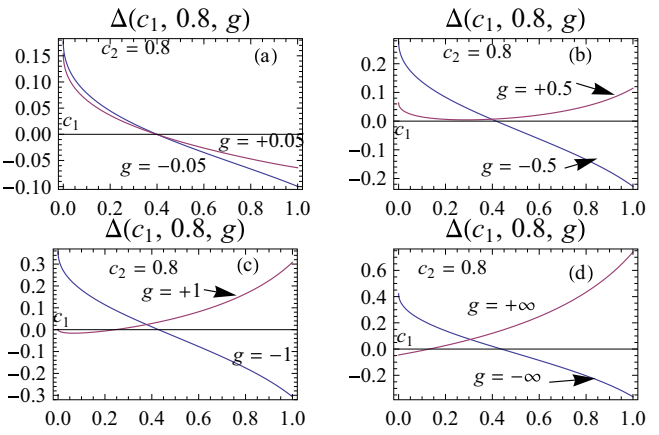

FIG. 16. (Color online) CAs (44) $\Delta(c_1, c_2, g)$ for the *asymmetric* BC $h_1 \neq h_2$, with c_2 arbitrarily fixed as $c_2 = 0.8$ just as in Fig. 13(b). Plots are given for (a) smaller values of the field $g = \pm 0.05$, which refers to the linear regime of the GB, (b) $g = \pm 0.5$, (c) $g = \pm 1$, and (d) $g = \pm\infty$. Curves $\Delta(c_1, c_2, \pm g)$ are close to each other for small $|g|$, just as in Fig. 14. However, unlike the symmetric BC, CAs presently take both positive and negative values. As the strength g grows larger, curves $\Delta(c_1, 0.8, g)$ and $\Delta(c_1, 0.8, -g)$ split more and more up to limiting cases $g = \pm\infty$, behaving in the reverse order $\Delta(c_1, 0.8, g)\Delta(c_1, 0.8, -g) < 0$ regarding their nature on a significant part of the interval of the variable $c_1 \in [0,1]$, yet perceptibly narrower in case (d) than in Fig. 15(b) for *symmetric* BC.

Figures 16(b)–16(d) examine CAs for (ii) antisymmetric BCs by gradually increasing the field g up to the limiting cases $g = \pm\infty$, also illustrating the tendency of curves $\Delta(c_1, c_2 = 0.8, g)$ and $\Delta(c_1, c_2 = 0.8, -g)$ to split for larger values of g outside the linear regime, just in analogy with the case in Fig. 15. The inequality $\Delta(c_1, 0.8, g)\Delta(c_1, 0.8, -g) < 0$ although valid on the significant part of the interval of the variable c_1 is yet restricted on the narrower subinterval [Fig. 16(d)] than in the symmetric case [Fig. 15(b)].

While the nature of CAs (i) $\Delta(c_1 = c_2, g \ll 1)$ and (ii) $\Delta(c_1, c_2 = 0.8, g \ll 1)$ are crucially different in the linear regime of g, $g \ll 1$ [cf. Figs. 14 and 16(a)], these quantities become *qualitatively* similar for *larger* values of the GB strength g, which *dominates notably over the influence of surface fields* h_1, h_2 [cf. Figs. 15 and 16(b)–16(d)], although naturally quantitative variations between them are clearly discernible.

V. CONCLUSIONS

We have scrutinized *exactly* the full form of universal functions of EDPs together with analysis of their short-distance expansion in Ising strips confined by two symmetry-breaking "surfaces" characterized by variable surface fields variables $y_i = D^2 h_i^2 L$ $(i = 1,2)$. Intriguing crossover behaviors of either EDPs, CAs, or distant-wall correction universal amplitudes mentioned in Sec. III emerge from the new characteristic length l_1 (3) in the critical system besides the film width L.

After identification of surface exponents we have perceived a distant-wall correction with the structure and surface exponent essentially referring to dGF amplitude (31) and therefore likely connected with the stress-tensor component perpendicular to the surface $T_{\perp\perp}(\vec{r}_{||},z\to 0)$ [cf. Eqs. (23)–(25)]. The discovery of the *generalized* form of dGF amplitude under freely variant BCs (31) within this study, is an extraordinary feature taking into account that the conformal invariance symmetry is broken for such BCs. The study of the structure of the distant-wall correction associated with dGF amplitude which itself is linked with CA [cf. Eqs. (28), (30), and (31)] required that I undertake independent analysis of the critical Casimir force using the current method. CAs $\Delta(y_1,y_2)$ controlled only by surface fields exhibit exciting complex crossover behavior, showing that the Casimir force can be so tuned that it becomes attractive, repulsive, or even switched off from the confined strip along certain trajectories in the (c_1,c_2) plane.

We have also examined in Sec. IV the more complicated physical situation when, apart from surface fields, the confined Ising strip also has the internal GB. The simultaneous influence of variable BCs and the GB brings in new effects dramatically affecting both EDPs and CAs. While the nonmonotonicity of EDPs remains their main feature near confining surfaces for finite values of surface fields variables $0<y_i<+\infty\,(i=1,2)$, the GB brings about crucial changes in their overall behavior, making them more positive or negative, increasing or decreasing their amplitudes and controlling their diverging behavior near the GB according to the law (34).

In connection with standard surface universality classes using the present theoretical framework I have derived closed analytic solutions for EDPs $\varepsilon_{\rm NN}(x,g)$, $\varepsilon_{\rm OO}(x,g)$, and $\varepsilon_{\rm NO}(x,g)$. These formulas, besides giving us insight into their detailed behavior, asymptotic limits, etc., reveal a few symmetry properties (39), (40), and (43) that may generally have pervasive consequences [57] on the Casimir effect for standard BCs with the internal GB.

The behavior of CAs $\Delta(y_1,y_2,g)$ via the broad interplay of tunable surface fields and the GB is inspected in detail. The GB strongly alters both the nature and magnitude of the Casimir force with respect to the case without GB. As a rule manifolds $\Delta(y_1,y_2,g)$ of CAs for lower values of the GB strength $g\in(g_2^\star\simeq-0.235,g_1^\star\simeq 0.246)$, in particular in the linear regime, $g\ll 1$ become qualitatively similar to the unperturbed case $(g=0)$ in Fig. 2, although CAs may still acquire prominently larger positive and negative values than before. Crossover behavior of CAs for larger values of the GB field $|g|$ is definitely very different from the unperturbed case $g=0$ in Fig. 2. Figures 9(a), 10(a), and 11 characterize CAs in this regime of larger g comprising single areas of positive and negative values delimited by the sole line of zeros $\Delta(c_1^\star,c_2^\star,g)=0$. At the same time with the growing field $|g|$ CAs $\Delta(c_1,c_2,g)$ may acquire more than ten times larger limiting values than in the unperturbed case (22). CAs $\Delta(c_1,c_2,g=-\infty)$ [cf. Fig. 11(a)] and $\Delta(c_1,c_2,g=+\infty)$ [cf. Fig. 11(b)] are *near* symmetric with respect to the axis $c_1+c_2=1$. Roughly similar correspondence may hold in some proportion even for lower values of $|g|$, as in Figs. 9(a) and 10(a).

To further elucidate the role of the GB onto the Casimir effect and single out its peculiar influence from surface fields, I have explored the CAs as the function of the field g in two most characteristic cases for (i) *symmetric* $(h_1=h_2)$ and (ii) *asymmetric* $(h_1\neq h_2)$ BCs. I have determined that CAs qualitatively remain similar to the unperturbed case in the linear regime $|g|\ll 1$: (i) $\Delta(c_1=c_2,g\ll 1)$ is always *negative* (cf. Fig. 14), while (ii) $\Delta(c_1\neq c_2,g\ll 1)$ may be both *positive* and *negative* [cf. Fig. 16(a)]. However, larger values of the GB field $|g|$ incline to cancel out to some extent differences between cases (i) and (ii), as Figs. 15 and 16(b)–16(d) show. I have also shown that in the domain of large g, $|g|\gg 1$, CAs $\Delta(c_1,c_2,g)$ and $\Delta(c_1,c_2,-g)$ tend to split mutually so as that they behave contrary to each other regarding the nature of the Casimir force: It holds almost everywhere on $c_1\in(0,1)$ for finite and infinite $|g|\gg 1$ that $\Delta(c_1=c_2,g)\Delta(c_1=c_2,-g)<0$ for *symmetric* BC $(h_1=h_2)$ [see Figs. 15(a) and 15(b)], while the same inequality remains valid for *asymmetric* BC to a significant extent, in particular for $|g|\to\infty$ [see Figs. 16(b)–16(d)]. These findings also complement the above discussion on the near-symmetry between CAs $\Delta(c_1,c_2,g)$ and $\Delta(c_1,c_2,-g)$ for larger GB fields $|g|$ in Fig. 11.

It is a result of many studies so far that Casimir interaction may be tuned either by BCs or by changing the temperature [8,9,51–53]. This report deals with the possibility when general smoothly varying BCs affect EDPs and CAs. A recent experiment demonstrated that critical Casimir forces in colloidal systems can be continuously tuned [58] by the choice of BCs. By measuring the interaction potential of the colloid particle in the mixture of water and 2,6-lutidine above the substrate with the gradient it was shown that it may change from attraction to repulsion even for small changes in the surface properties. These experimental findings are fully in accord with results of the present work demonstrating the possibility to continuously change the critical Casimir force by smooth variation of BCs. It was recognized that Casimir forces sensitive to surface properties bring in novel perspectives of colloidal suspensions as model systems [58]. On the other hand, it was suggested that this also opens new possibilities for fabrication of colloidal crystals which are significantly important for technical applications.

Besides tunable BCs and thermal adjustments, an additional possibility to influence the Casimir force arises with the GB present in the critical system as the current study examines. I have elucidated how the EDP as order parameter of the system as well as CAs may be altered by the GB. Both the nature of the Casimir force (repulsive or attractive) and its magnitude may undergo compelling changes due to the impact of the GB. Besides the fundamental importance, this may also be applied to real materials and to engineering their desirable properties.

The present study can be extended to higher dimensions [59] $d>2$, as well as to confined layered Ising models, etc. Consequently, new effects in higher dimensions may be expected, such as the presence of the (SB) fixed point and the possibility to examine the important case of the XY model relevant to ^{4}He near the λ point of superfluid transition if (OO) BCs are imposed. The fact that the present model is applicable in $2\leqslant d\leqslant 4$ for arbitrary BCs is an advantage over transfer-matrix methods $(d=2)$. Additionally, it may be preferred over the standard field-theoretic method [1], confined *only* to the mean-field limit [12] for symmetry-breaking BCs.

ACKNOWLEDGMENT

I acknowledge financial support for this work from the Serbian Ministry of Education, Science and Technological Development through Project No. 171015.

APPENDIX: EDPs FOR (NN) AND (OO) BCs WITH THE GB

We derive here analytic solutions of EDPs for (NN) and (OO) BCs. The integration (12) of energy-density modes $\varepsilon_q^{\rm NN}(x,g)$, defined by Eq. (37), may be carried out in terms of Gaussian hypergeometric function [60,61] ${}_2F_1(a,b,c,z)$. Using the *regularized Gaussian hypergeometric* function ${}_2\tilde{F}_1(a,b,c,z) := {}_2F_1(a,b,c,z)/\,\Gamma(c)$, with $\Gamma(c)$ as the Γ function, I recast the original very lengthy solution to a somewhat more compact form:

$$
\begin{aligned}
L\varepsilon_{\rm NN}(0<x<1/2,g) = \frac{1}{16}\exp(-g)\Bigg\{ & \frac{2\Gamma(1-2x)}{\pi}\Bigg[\frac{1}{\exp(2g)+1}\Bigg((1+i\exp(g))(i+\exp(g))^3 \\
& \times {}_2\tilde{F}_1\left(1,1-2x,2(1-x);1-\frac{2}{1+i\exp(g)}\right)+i(\exp(2g)-1)(1-2x) \\
& \times\Bigg((\exp(g)-i)^2{}_2\tilde{F}_1\left(1,2(1-x),3-2x;1+\frac{2}{-1+i\exp(g)}\right) \\
& -(\exp(g)+i)^2{}_2\tilde{F}_1\left(1,2(1-x),3-2x,1-\frac{2}{1+i\exp(g)}\right)\Bigg)\Bigg) \\
& -i(\exp(g)-i)^2{}_2\tilde{F}_1\left(1,1-2x,2(1-x),1+\frac{2}{-1+i\exp(g)}\right)\Bigg] \\
& +\frac{1}{2\pi(1+x)}\Gamma(2(x+1))\Bigg[-2i(\exp(g)-i)^2{}_2\tilde{F}_1\left(1,2x+1,2(x+1),1+\frac{2}{-1+i\exp(g)}\right) \\
& +\frac{(1+i\exp(g))(\exp(g)-1)(\exp(g)+1){}_2\tilde{F}_1\left(1,2x,2x+1;1+\frac{2}{-1+i\exp(g)}\right)}{(\exp(g)+i)x} \\
& +2i(\exp(g)+i)^2{}_2\tilde{F}_1\left(1,2x+1,2(x+1);1-\frac{2}{1+i\exp(g)}\right) \\
& +\frac{(1-i\exp(g))(\exp(g)-1)(\exp(g)+1){}_2\tilde{F}_1\left(1,2x,2x+1,1-\frac{2}{1+i\exp(g)}\right)}{(\exp(g)-i)x}\Bigg]\Bigg\}. \qquad \text{(A1)}
\end{aligned}
$$

The second branch of the solution $\varepsilon_{\rm NN}(-1/2<x<0,g)$ arises from Eq. (A1) because $\varepsilon_{\rm NN}(x,g)$ is an even function of the argument x due to the symmetry of (NN) BC. Graphs of the EDP $\varepsilon_{\rm NN}(x,g)$ obtained from Eq. (A1) are given by Figs. 8(e) and 8(f) for a couple of strengths $g=0.1,-2$.

Similarly integrating energy density modes $\varepsilon_q^{\rm OO}(x,g)$ defined by Eq. (38) in Eq. (12), I obtain the analytic solution for EDP for the (OO) BC conveniently presented in terms of regularized Gaussian hypergeometric function ${}_2\tilde{F}_1(a,b,c,z)$:

$$
\begin{aligned}
L\varepsilon_{\rm OO}(0<x<1/2,g) = \frac{1}{8}\Bigg\{ & \frac{\Gamma(2(1+x))}{2\pi(1+x)}\Bigg[2(1-i\sinh(g)){}_2\tilde{F}_1\left(1,2x+1,2(x+1);-1-\frac{2i}{-i+\exp(g)}\right) \\
& +\frac{1}{(\exp(2g)+1)x}\exp(g)\Bigg[{}_2\tilde{F}_1\left(1,2x,2x+1,-1-\frac{2i}{-i+\exp(g)}\right)(2\sinh(g)-i\cosh(2g)+i) \\
& +2(1+i\sinh(g))\Bigg(\sinh(g){}_2\tilde{F}_1\left(1,2x,2x+1,\frac{2i}{i+\exp(g)}-1\right) \\
& +2x\cosh(g){}_2\tilde{F}_1\left(1,2x+1,2(x+1);\frac{2i}{i+\exp(g)}-1\right)\Bigg)\Bigg]\Bigg] \\
& -\frac{2i\Gamma(2(1-x))}{\pi}\Bigg[\frac{1}{\exp(2g)+1}\sinh(g)\Bigg((\exp(g)+i)^2{}_2\tilde{F}_1\left(1,2(1-x),3-2x;-1-\frac{2i}{-i+\exp(g)}\right) \\
& -(\exp(g)-i)^2{}_2\tilde{F}_1\left(1,2(1-x),3-2x;\frac{2i}{i+\exp(g)}-1\right)\Bigg)
\end{aligned}
$$

$$+\frac{(\sinh(g)-i)_2\tilde{F}_1\left(1,1-2x,2(1-x);-1-\frac{2i}{-i+\exp(g)}\right)}{2x-1}$$
$$+\frac{(\sinh(g)+i)_2\tilde{F}_1\left(1,1-2x,2(1-x);-1-\frac{2i}{-i+\exp(g)}\right)}{1-2x}\Bigg]\Bigg\}. \quad \text{(A2)}$$

Again I avoid explicitly quoting the second branch of the solution for the EDP for (OO) BC $\varepsilon_{\rm OO}(-1/2<x<0,g)$ as it follows from Eq. (A2) due to the symmetry of (OO) BC, which imposes parity relation $\varepsilon_{\rm OO}(-x,g)=\varepsilon_{\rm OO}(x,g)$. Plots of $\varepsilon_{\rm OO}(x,g)$ derived by means of Eq. (A2) are presented in Figs. 8(a)–8(d) for GB fields $g=\pm 0.1,\pm 5$.

[1] H. W. Diehl, in *Phase Transitions and Critical Phenomena*, edited by C. Domb and J. L. Lebowitz (Academic Press, London, 1986), Vol. 10.

[2] Here I briefly define (E, O, SB) BCs. The (E) BC designates already ordered surface in the presence of the bulk system above the bulk critical temperature T_c. It is generally accepted that such situation is equivalent to the surface being exposed to the infinite surface magnetic field $h_1=+\infty$, which is then called the *normal* (N) surface universality class. The (O) BC refers to the confining surface that has not ordered spontaneously yet and therefore it does not break the O(N) symmetry of the bulk spin system ($N=2$ for the Ising universality class). I refer to such kind of BCs as *symmetry preserving*. The (O) BC is modeled by the zero surface magnetic field $h_1=0$ for all temperatures above the critical temperature $T_{c,S}$ of the surface spontaneous ordering. The (SB) phase transition describes simultaneous ordering of the bulk and the surface. It is a multicritical end point of (O) and (E) phase transitions. I define changeable BCs in this paper by such surface magnetic fields $h_i (i=1,2)$ that they may take intermediate values $0<h_i<+\infty$ with respect to the limiting values $h_i=0 h_i=+\infty$ for (O) and (N) surface universality classes, respectively.

[3] U. Ritschel and P. Czerner, Phys. Rev. Lett. **77**, 3645 (1996); A. Ciach and U. Ritschel, Nucl. Phys. B **489**, 653 (1997).

[4] E. Brézin and S. Leibler, Phys. Rev. B **27**, 594 (1983).

[5] L. Mailänder, H. Dosch, J. Peisl, and R. L. Johnson, Phys. Rev. Lett. **64**, 2527 (1990).

[6] N. S. Desai, S. Peach, and C. Franck, Phys. Rev. E **52**, 4129 (1995).

[7] J.-H. J. Cho and B. M. Law, Phys. Rev. Lett. **86**, 2070 (2001).

[8] M. Krech, *Casimir Effect in Critical Systems* (World Scientific, Singapore, 1994).

[9] A. Gambassi, J. Phys: Conf. Ser. **161**, 012037 (2009); M. Krech, J. Phys.: Condens. Matter. **11**, R391 (1999).

[10] F. M. Schmidt and H. W. Diehl, Phys. Rev. Lett. **101**, 100601 (2008).

[11] D. B. Abraham and A. Maciołek, Phys. Rev. Lett. **105**, 055701 (2010); P. Nowakowski and M. Napiorkówski, Phys. Rev. E **78**, 060602(R) (2008).

[12] T. F. Mohry, A. Maciołek and S. Dietrich, Phys. Rev. E **81**, 061117 (2010).

[13] L. V. Mikheev and M. E. Fisher, Phys. Rev. Lett. **70**, 186 (1993); Phys. Rev. B **49**, 378 (1994).

[14] T. W. Burkhardt and T. Xue, Phys. Rev. Lett. **66**, 895 (1991); Nucl. Phys. B **354**, 653 (1991).

[15] J. L. Cardy, in *Phase Transitions and Critical Phenomena*, edited by C. Domb and J. L. Lebowitz (Academic Press, London, 1987), Vol. 11.

[16] J. L. Cardy, Phys. Rev. Lett. **65**, 1443 (1990).

[17] S. Dietrich, in *Phase Transitions and Critical Phenomena*, edited by C. Domb and J. L. Lebowitz (Academic Press, London, 1988), Vol. 12.

[18] R. Kikuchi and J. W. Cahn, Phys. Rev. B **21**, 1893 (1980).

[19] D. B. Abraham, Phys. Rev. Lett. **44**, 1165 (1980); J. Phys. A: Math. Gen. **14**, L369 (1981).

[20] D. B. Abraham and N. M. Švrakić, J. Phys. A: Math. Gen. **19**, L599 (1986).

[21] G. Bilalbegović, J. Stat. Phys. **50**, 1131 (1988).

[22] A. Sevrin and J. O. Indekeu, Phys. Rev. B **39**, 4516 (1989).

[23] F. Iglói and J. O. Indekeu, Phys. Rev. B **41**, 6836 (1990).

[24] D. B. Abraham, V. Mustonen, and A. J. Wood, Phys. Rev. Lett. **93**, 076101 (2004); Phys. Rev. E **71**, 036106 (2005).

[25] D. B. Abraham, V. Mustonen, and A. J. Wood, Phys. Rev. E **70**, 066138 (2004).

[26] B. Chopard and M. Droz, *Cellular Automata Modelling of Physical Systems* (Cambridge University Press, Cambridge, UK, 1998); J. Marro and R. Dickman, *Nonequilibrium Phase Transitions in Lattice Models* (Cambridge University Press, Cambridge, UK, 1999); H. Hinrichsen, Adv. Phys. **49**, 815 (2000); U. C. Täuber, Adv. Solid. State. Phys. **43**, 659 (2003).

[27] T. Vojta, Phys. Rev. E **70**, 026108 (2004).

[28] P. Wynblatt and Z. Shi, J. Matter. Sci. **40**, 2765 (2005).

[29] J. M. Rickman, H. M. Chan, M. P. Harmer, and J. Luo, Surf. Sci. **618**, 88 (2013).

[30] J. S. Rowlinson and B. Widom, *Molecular Theory of Capillarity* (Clarendon, Oxford, UK, 1982).

[31] Generally, the functional in the theory of critical phenomena is called *local* when, e.g., it is given as a spatial integral over the finite number of fields or densities $m(\vec{r})$ and their simple derivatives $\nabla m(\vec{r})$, $\nabla^2 m(\vec{r})$, ...

[32] M. E. Fisher and P. G. de Gennes, C. R. Séances Acad. Sci. Sér. B **287**, 207 (1978).

[33] M. E. Fisher and P. J. Upton, Phys. Rev. Lett. **65**, 3405 (1990).

[34] S.-y. Zinn and M. E. Fisher, Phys. Rev. E **71**, 011601 (2005).

[35] Z. Borjan and P. J. Upton, Phys. Rev. E **63**, 065102 (2001).

[36] Z. Borjan and P. J. Upton, Phys. Rev. Lett. **81**, 4911 (1998).

[37] L. V. Mikheev and M. E. Fisher, J. Stat. Phys. **66**, 1225 (1992).

[38] M. Krech, E. Eisenriegler, and S. Dietrich, Phys. Rev. E **52**, 1345 (1995).

[39] E. Eisenriegler, M. Krech, and S. Dietrich, Phys. Rev. B **53**, 14377 (1996).
[40] T. W. Burkhardt and E. Eisenriegler, Nucl. Phys. B **424**, 487 (1994).
[41] T. W. Burkhardt and E. Eisenriegler, J. Phys. A: Math. Gen. **18**, L83 (1985).
[42] M. P. Nightingale and J. O. Indekeu, Phys. Rev. Lett. **54**, 1824 (1985).
[43] O. Vasilyev, A. Maciołek, and S. Dietrich, Phys. Rev. E **84**, 041605 (2011).
[44] H. Au-Yang and M. E. Fisher, Phys. Rev. B **11**, 3469 (1975).
[45] J. L. Cardy, Nucl. Phys. B **275**, 200 (1986).
[46] H. W. J. Blöte, J. L. Cardy, and M. P. Nightingale, Phys. Rev. Lett. **56**, 742 (1986); I. Affleck, *ibid.* **56**, 746 (1986).
[47] T. W. Burkhardt and J. L. Cardy, J. Phys. A: Math. Gen. **20**, L233 (1987).
[48] E. Eisenriegler, M. Krech, and S. Dietrich, Phys. Rev. Lett. **70**, 619 (1993).
[49] T. W. Burkhardt and I.-Y. Choi, Nucl. Phys. B **376**, 447 (1992).
[50] Here I denote BC for infinite values of surface field variables $y_1 \to \infty$, $y_2 \to \infty$ as $(++)$.
[51] R. Evans and J. Stecki, Phys. Rev. B **49**, 8842 (1994).
[52] Z. Borjan and P. J. Upton, Phys. Rev. Lett. **101**, 125702 (2008).
[53] M. Krech, Phys. Rev. E **56**, 1642 (1997).
[54] J. Milnor, *Singular Points of Complex Hypersurfaces* (Princeton University Press, Princeton, NJ, 1969).
[55] A singular point of a real curve $F(x,y) = 0$ is a point (x_0, y_0) at which the first partial derivatives vanish $(F'_x)_0 = 0$, $(F'_y)_0 = 0$. The nodal singularity is a point of intersection of smooth branches of the curve.
[56] Let $\Phi(c_1, \Delta, g) = 0$ be a family of single-parameter curves. Then there are points K when the two infinitesimally close curves of the family, given by parameters g and $g + \Delta g$, are at closest distances. These are either intersection points on (g) and $(g + \Delta g)$ or points on (g) the distance of which from $(g + \Delta g)$, along the perpendicular line, is an infinitesimal quantity of the higher order than Δg. When $\Delta g \to 0$ the curve $(g + \Delta g)$ comes near the curve (g) while the point K may sometimes verge to the limiting position, which is then called the characteristic point. Singular points (such as intersection, isolated, or cusp points or the point of osculation) are always characteristic points.
[57] Z. Borjan (unpublished).
[58] U. Nellen, L. Helden, and C. Bechinger, Europhys. Lett. **88**, 26001 (2009).
[59] L. V. Mikheev, Phys. Rev. B **50**, 3869 (1994).
[60] M. Abramowitz and I. A. Stegun, *Handbook of Mathematical Functions*, 9th ed. (Dover, New York, 1972).
[61] W. Becken and P. Schmelcher, J. Comput. Appl. Math. **126**, 449 (2000).